# Journal Pre-proof

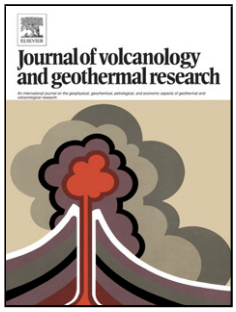


Comparative field study of shallow rhyolite intrusions in Iceland: emplacement mechanisms and impact on country rocks

Elodie Saubin, Ben Kennedy, Hugh Tuffen, Marlene Villeneuve, Jonathan Davidson, Steffi Burchardt

PII: S0377-0273(19)30350-6

DOI: https://doi.org/10.1016/j.jvolgeores.2019.106691

Reference: VOLGEO 106691

To appear in:

Received Date: 28 June 2019

Revised Date: 16 October 2019

Accepted Date: 20 October 2019

Please cite this article as: Saubin E, Kennedy B, Tuffen H, Villeneuve M, Davidson J, Burchardt S, Comparative field study of shallow rhyolite intrusions in Iceland: emplacement mechanisms and impact on country rocks, *Journal of Volcanology and Geothermal Research* (2019), doi: https://doi.org/10.1016/j.jvolgeores.2019.106691

# Comparative field study of shallow rhyolite intrusions in Iceland: emplacement mechanisms and impact on country rocks

Elodie Saubin[1], Ben Kennedy[1], Hugh Tuffen[2], Marlene Villeneuve[1], Jonathan Davidson[1], Steffi Burchardt[3]

[1] Department of Geological Sciences, University of Canterbury, Ilam road, Christchurch 8041, New Zealand

[2] Lancaster Environment Centre, Lancaster University, Lancaster, UK

[3] Department of Earth Science, Uppsala University, Uppsala, Sweden

Corresponding author: elodie.saubin@pg.canterbury.ac.nz

HIGHLIGHTS

- Four rhyolite intrusions in Iceland are extensively described with insights on the interface and on damaged country rocks
- A TinyPerm and Schmidt hammer permitted in-field characterisation of rock properties
- Weak and porous conglomerate and hyaloclastite react to the intrusions by pore occlusion, with reduced permeability
- Strong basalt lava and welded ignimbrite are weakened by the intrusions, with additional fractures, and cut by tuffisite veins

## Abstract

Shallow silicic intrusions are known to exist in many active volcanoes and can fuel both eruptions and hydrothermal fields. However, our knowledge of magma intrusions remains far from complete, and processes occurring at intrusion margins are poorly understood. In this field-based study, we characterise four shallows, dissected rhyolitic intrusions at three sites in Iceland (Njarðvík-Dyrfjöll, Krafla and Húsafell central volcanoes). We focus on the relationship between intrusion emplacement mechanisms and country rock response, employing scanline mapping of fractures and in-situ rock property measurements (hardness and permeability) along transects from the intrusion margins to damaged and undamaged country rocks.

We identify various scenarios of shallow intrusion emplacement style, based upon their diverse geometry and lithofacies architecture. Additional information from rock properties and

characteristics of fractures and vesicles, indicates that initial country rock properties strongly influence the emplacement style. We identify two discrete types of country rock response to magma injection. The matrix permeability of weak, porous and permeable lithologies (conglomerate and hyaloclastite) is reduced by >1 order of magnitude adjacent to intrusions due to pore occlusion. Stronger and denser, low-permeability lithologies (basalt and welded ignimbrite) undergo a decrease in hardness by a factor >2 related to an up to fivefold increase in fracture density, with no significant change in matrix permeability.

Our observations highlight the importance of robust characterisation of the mechanical properties of caldera-filling or geothermal reservoir formations, for appropriate forecasting of magma mobility, geophysical data interpretation, and geothermal resources characterisation.

Keywords: Rhyolite. Intrusion. Iceland. Damage. Emplacement. Permeability

## 1. Introduction

Magmatic activity in Iceland is dominantly basaltic in composition (Walker, 1966; Sigurdsson, 1977; Thordarson and Larsen, 2007). However, rhyolitic magma is generated at central volcanoes by partial melting of altered basaltic crust and/or fractional crystallisation (e.g. Jónasson, 1994; Gunnarsson et al., 1998), producing rhyolites with higher temperatures and lower viscosity compared to subduction zone rhyolites (Zierenberg et al., 2012; Reid, 1983). These intrusive complexes become the shallow roots of some of the most vigorous hydrothermal systems, used for geothermal energy production in Iceland (e.g. Krafla). Supercritical fluids suitable for powerful energy extraction can be stored at the margins of the intrusions (40-50 MWe per well; Albertsson et al., 2003), where rock properties likely control both eruption and energy potential (e.g. Lamur et al., 2017, Eggertsson et al., 2018, Mordensky et al., 2018a and b).

Processes related to magma transport in volcanic plumbing systems are the subject of active research, illustrated in recent studies reviewing melt segregation, emplacement and storage systems (e.g. Holness, 2018; Healy et al., 2018). Magma emplacement style depends on physical properties and structure of surrounding rocks, regional tectonics and magma rheology (Pollard, 1973; Spence and Turcotte, 1985; Hutton, 1988; Clemens and Petford, 1999; Galland et al., 2006; Matsson et al. 2018; Stephens et al., 2018; Burchardt et al. 2019). As examples, transition from a dyke to a sill is associated to a variation of strength in layered country rocks (Kavanagh et al. 2006; Maccaferri et al., 2011) and/or to the occurrence of a strong compressive tectonic stress (Gudmundsson., 1990; Maccaferri et al., 2011), and the intrusion width is affected by the country rock lithology and magma viscosity (e.g. Krumbholz et al. 2014).-Propagating magma exploits pre-

existing discontinuities in country rock (Lamur et al., 2017; Le Corvec et al., 2013), but also creates new fractures at the tips, with hydraulic tensile fracturing or shear faulting (Mathieu et al., 2008; Kavanagh, 2018). The opening direction of intrusions is therefore a result of stresses and country-rocks properties (Kavanagh, 2018). These fracturing processes include the formation of tuffisite veins, which open pathways for silicic magma to propagate, degas, and erupt (e.g. Stasiuk et al., 1996; Tuffen and Dingwell, 2005; Saubin et al., 2016). They form by exsolved magmatic gas that inject into fractures within country rocks (Heiken et al., 1988). Continued propagation of pressurised magmatic fluids can widen the veins, facilitating magma emplacement (Stasiuk et al., 1996; Tuffen and Dingwell, 2005; McGowan, 2016).

Besides fracturing occurring at the intrusive tips, country rocks can be locally deformed and fractured along the contacts (Kavanagh and Sparks, 2011). Strong, low-porosity material undergoes limited elastic or inelastic deformation response to pressure increase associated with intrusion, leading to material failure (e.g. Paterson et al., 1996). In contrast, weak, porous units favour the circulation of hot fluids causing thermal alteration and thermal fracturing, and will undergo significant ductile deformation with shear failure (Delaney et al., 1986; Wong and Baud, 2012; Mordensky et al., 2019). Within the intrusion, small-scale (millimetre) perlitic fracture networks can develop in quenched glassy margins (von Aulock et al., 2013), facilitating significant ingress of external water. In the country rock at the immediate vicinity of the intrusion, the high fracture density is associated with permeability increase. This may create conditions suitable for a geothermal resource with circulation of high-enthalpy fluids (e.g. Carrigan; 1986; Paterson et al., 1996; Scott et al., 2017; Mordensky et al., 2018a, 2018b).

Magma propagation and country rock response elucidate textural, as well as structural adjustments. High internal shear stress and rapid quenching at the contact can form platy jointing (Conway et al., 2015; Magnall et al., 2018). Contact-parallel flow colour banding can occur in the glass, reflecting variable cooling rates, incremental pulses of magma emplacement, or shear-driven crystal variation (Tuffen and Castro, 2009; McGowan, 2016; Mattsson et al., 2018). These magma flows can be associated with decompression, which causes melt to degas through vesicle nucleation and growth (e.g. Hamada et al., 2010). Parameters impacting this magma response include the decompression rate, magma viscosity, volatile content and quench rate (e.g. Sparks, 1978; Papale et al., 1998; Shea et al., 2010; von Aulock et al., 2017). The melt flow deforms vesicles according to the strain rate, which changes depending on the velocity gradient across the intrusion (e.g. Rust et al., 2003; Okumura et al., 2009; Dingwell et al., 2016). Secondary changes may be caused by coalescence, outgassing or relaxation, and a pumiceous foam can form for highly-vesicular magma, then fragment or collapse (Westrich et al., 1988; Okumura et al., 2006; Kennedy et al., 2016). Vesicle size distribution can consequently be an indicator of degassing

processes, and vesicle shapes and orientations can record processes related to stress and flow direction (e.g. Sparks, 1978; Stasiuk et al., 1996; Manga et al., 1998; Shea et al., 2010; Toramaru, 2014; Dingwell et al., 2016; Wadsworth et al., 2017).

The heat transfer to the country rock and the related hydrothermal alteration are dominantly controlled by intrusion thickness (e.g. Annen, 2017). Heat transfer can be associated with heat convection or advection by hydrothermal fluids in presence of a developed fracture network (e.g. Parmentier and Schedl, 1981; Huppert et Sparks, 1989). Hot aqueous fluids drive mineralogical, chemical and textural changes in the rock, with released oxygen causing oxidation and thus colour change, together with iron leaching (e.g. Pirajino, 2008). Heating of the country rock can cause dehydration of mineral species, reactions between minerals, or dissolution (e.g. Galushkin, 1997; Siratovich et al., 2011; Farquharson et al., 2018; Mordensky et al., in press). Despite the importance of these processes in country rock alteration, chemical impacts of intrusions are beyond the scope of this study.

This paper presents field case studies of four fossil rhyolitic intrusions from three shallow plumbing systems in Iceland. Rock mass properties are investigated in and around similar dimension intrusions, within distinct country rocks. Vesicle populations in intrusions record cooling, degassing and emplacement processes, whereas field estimates of rock hardness, permeability and fracture density in country rocks indicate the mechanical and thermal impacts of intrusion at the interface. We conceptualise the influence of the country rock and intrusion style on the emplacement, degassing, and geothermal potential of rock masses surrounding shallow rhyolite intrusions.

## 2. Methodology

The field areas (Fig. 1) all comprise one or more shallow rhyolite body, intruded within diverse country rock lithologies. These sites were chosen to represent similar intrusion compositions, dimensions and emplacement depths, at relatively unweathered and accessible outcrops. We conducted qualitative and quantitative assessment of intrusion dimensions, geometries, and vesicle populations including density, size and orientation. In the country rocks, information were primarily collected in the damaged zone, but also in the undamaged country rock away from the intrusion as a control. It concerns the lithofacies architecture, rock properties including hardness and permeability, and details of fracture populations such as density, size and orientation. The term “damaged zone” in this study refers to both hydrothermal alteration and intrusion-triggered mechanical damage. Additional features at the interface such as tuffisite veins and brecciated

zones are also included in the descriptions. Figure S1 (Supplemental Material) shows the measurement locations.

### 2.1 3D photogrammetric reconstruction

Models of the three field areas were constructed from photography using the structure from motion (SfM) photogrammetric technique in the Agisoft Photoscan (Metashape) software. Images were collected using either an unmanned aerial vehicle (UAV; DJI phantom 3), or a combination of both the UAV and a handheld camera. The UAV photographs were geo-tagged using a standard GPS and the final models have a ~3 m RMS error in location, with resolution of ~10 mm/pixel. They are used to approximate the three-dimensional intrusion geometries (Figs. 2, 3, 4). Contacts and faults orientation were measured in-the field with a compass clinometer, constraining the 3D models. Compass measurements were corrected with 10° of declination at Njarðvík-Dyrfjöll (Landsendi outcrop), 11° at Krafla (Hrafntinnuhryggur outcrop) and 13° at Húsafell (West and East outcrops), appropriate for the date of fieldwork in 2017 and 2018.

### 2.2 Rock properties

Permeability and hardness are estimated in the field with the respective use of TinyPerm (Farquharson et al., 2015) and Schmidt hammer (Aydin and Basu, 2005). Although such field techniques lack the accuracy of equivalent laboratory measurements, they permit collection of large in-situ datasets and can be used to reflect relative spatial variation within the outcrop (Mordensky et al., 2018b).

The TinyPerm is a portable air permeameter used perpendicular to smooth surfaces. Air is drawn through the volume of rock adjacent to the nozzle, with a vacuum initially created at the nozzle-rock interface (Mordensky et al., 2018b). The permeability calculation is described in Brown and Smith (2013). The use of the TinyPerm is validated by laboratory measurements of permeability on a heterogeneous block of hyaloclastite from the field site of Krafla (Fig. 1), which provided the same range of relative values to the field permeameter results, with natural variability of half an order of magnitude (Eggertson et al., 2018). Absolute values should however be considered as approximate, with uncertainties ± 5 % (Brown and Smith, 2013). We differentiate in this paper the matrix permeability measured with the TinyPerm and the rock mass permeability, which takes into account fractures and lithological structures.

Field rock hardness was determined using a type-L Schmidt hammer, requiring a minimum of 10 measurements at each location (ASTM, 2001). The final value is calculated from the average, as suggested in Amaral et al. (1999). The inbuilt spring-driven piston is released on a rock surface, and a correlation chart relates the registered rebound value to rock strength (e.g. Deere and Miller,

1966; del Potro and Hürlimann, 2008; Mordensky et al., 2018b). The absolute values of strength are however not well constrained for these rocks, and rock hardness measurements assess relative spatial variation only. Laboratory measurements of Uniaxial Compressive Strength (UCS) were performed by Eggertson (2019) on two Icelandic rocks (dense basalt lava and hyaloclastite) among the four we encounter in this study.

Field conditions were highly variable (outcrop quality, dimensions and accessibility). Despite efforts made to conduct consistent measurements, inter-site fluctuations were unavoidable. Measurements were recorded over two field seasons and the large number of scientists involved also impacts the data consistency. We focus our results on systematic measurements of rock properties conducted at ~5-10 cm intervals along 1-4 m long transects: 2 transects out of the 5 from Landsendi, 3 out of the 9 from Hrafntinnuhryggur, 1 from the 4 at Húsafell West, and the 2 from Húsafell East. Measurements were made on smooth surfaces free from water and lichen, avoiding macro-fractures. At each point, 1-6 good TinyPerm measurements (with smooth temporal decay of pressure differential) were recorded depending on time allocated per outcrop. We aimed for ~10 Schmidt hammer measurements close to the measurement points for the TinyPerm. As Schmidt hammer rebound can damage the rock, permeability was measured first, and each rebound was conducted on a slightly different but adjacent surface. Results presented herein are calculated from the average of measurements for each point.

The lithologies are sorted according to the Geotechnical Classification of Volcanic Material procedure (GCVM, Del Potro and Hurliman, 2008), which includes the alteration and damage degree. Initially used for characterisation of material stability, it is also strongly related to drillability and relevant for geothermal.

**2.3 Fractures**

Our approach limits the permeability measurements to the rock matrix, as we intentionally avoided visible fractures. Rock mass permeability is considered through 1D mapping of spacing and dimensions of discontinuities, recorded using the simple scanline method in Manda and Mabee (2010). Scanline transects were typically 1-2 m in length, with >25 counted fractures, located in each lithology and across the contact in representative areas. Measurements concerned all discontinuity types (joints, bedding, faults, veins), their orientation, length and aperture, together with additional geometry factors and external effects (results can be made available on request). Average fracture density (number of fractures per metre) and average fracture area (length multiplied by aperture) were calculated for each country rock lithology.

Only a subset of the scanlines meets our need for a clear distinction between damaged and non-damaged country rock: 1 scanline out of the 6 from Landsendi, 3 out of the 11 from

Hrafntinnuhryggur, 2 out of the 4 from Húsafell West and the 2 from Húsafell East. At Landsendi, we used photos taken by a handheld camera at resolution of 1 mm/pixel to record fractures spacing, length and aperture along two additional transects, in locations inaccessible in the field. Higher resolution information on fracture density was collected at the best quality Húsafell West outcrop, where we counted the number of fractures over a 50 cm length parallel to the contact, repeating this measurement every 5-10 cm along the scanline transects. At Húsafell East, the two scanlines were completed with 6 photo-based transects to create a similar high-resolution fracture density profile (c.f. Supplemental Material, Fig.S1, Table S2).

### 2.4 Textures

Vesicularity was estimated at Landsendi using a vesicularity reference chart every ~2 m along the outcrop. At each site, the orientation, elongation and width of the biggest-sized vesicles were recorded every ~2-5 m along and across the intrusion, at the core, sill tips, top or bottom contact, and near features such as faults or internal rock deformation. The outcrop surfaces restrict the measurements to two-dimensions data. Vesicles size was measured with a mm-precision scale, resulting in resolution of 0.5 mm. Vesicles equivalent diameter (diameter of the rounded-shape vesicle of same area) and shape ratio (short axis divided by long axis) were calculated.

### 2.5 Statistical testing

We use the method of one-way analysis of variance (ANOVA; Fisher, 1925) to determine the significance of trends when those are unclear. It is the case for our permeability results, which variations within damaged country rocks are compared with variations in the undamaged rocks. The calculation compares the means of the two groups, taking into account their variance and resulting in an overall p-value (Miller and Rupert, 1997). The two groups are considered significantly different within the 95 % confidence interval when p-value $<0.05$. If p-value $>0.05$, the difference is not statistically significant. The data analysis for this study was generated using the Real Statistics Resource Pack software (Zaiontz, 2018).

## 3. Geological setting and description of intrusions

The three selected central volcanoes in Iceland are Njarðvík-Dyrfjöll, Krafla and Húsafell (Figure 1).

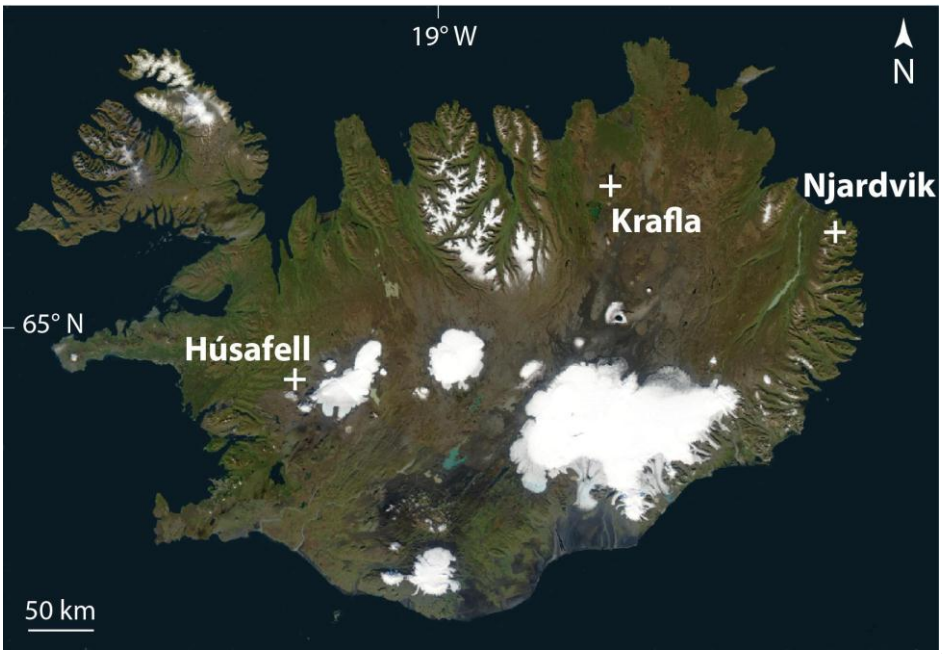


**Figure 1**. Map of central volcano field areas in Iceland (image from NASA). Refer to Table 1 for the outcrop coordinates.

### 3.1 Njarðvík-Dyrfjöll

The ~12 Ma Neogene Njarðvík-Dyrfjöll volcano in the East Fjords hosts an extensive system of rhyolitic dykes and sills. At the base of the exposed succession is a >300m thick sub-volcanic rhyolitic body cut by basaltic dykes. This is overlain by >500 m of basaltic lavas intruded by rhyolite (Gustafsson, 1992; Burchardt, 2008). The dykes extending from the rhyolitic intrusion at the base feed a ~100 m thick, irregular rhyolitic lava, which caps the basalt unit. Rhyolitic and basaltic intrusions crosscut each other, and indicate the existence of a source magma chamber near the centre of the caldera (Burchardt et al., 2011). The lens-shaped 1-4 m thick Landsendi sill is located on a peninsula east of the fjord Njarðvík, surrounded by fractured basaltic lavas (Fig. 2). Its emplacement depth is estimated at 500 m, indicated by the elevation of the coeval subaerial rhyolite lava higher in the sequence (Burchardt, 2008).

### 3.2 Krafla

The Krafla volcanic complex consists of a central caldera located in the northern rift zone of Iceland, associated with an elongate N-S trending fissure swarm (e.g. Thordarson and Larsen, 2007). Its activity is related to the rifting, with repeated inflation stages and subsidence events (Björnsson et al., 1979). The caldera is filled with basaltic hyaloclastites and lavas, whereas rhyolitic products are concentrated at and around the caldera rims. The last eruptions were basaltic and occurred between 1975-84 (e.g. Jónasson, 1994). Hrafntinnuhryggur is a dominantly obsidian ridge following the N-S fissure swarm trend, near the south-east rim of the Krafla caldera, formed in a small-volume rhyolitic fissure eruption at ~24 ka (Tuffen and Castro, 2009). At the south of the ridge, glacial erosion to ≤90 m beneath the syn-eruptive surface reveals a discordant

rhyolitic feeder dyke intruding basalts and hyaloclastites that are overlain by small, obsidian-rich lava bodies (Fig. 3).

### 3.3 Húsafell

Húsafell volcano in west Iceland was active 3–2.3 Ma ago (Saemundsson and Noll 1974), with three phases of silicic volcanism including the emplacement of significant volumes of ignimbrite. Numerous dykes, sheets, domes and vents were emplaced during the final silicic phase. They are extensively dissected in the valleys of Deildargil and Hringsgil, where these intrusions emplaced at ~500m depth and cut a series of conglomerates, ignimbrites and basaltic lavas (McGowan, 2016). The selected outcrops contain a rhyolitic intrusion of complex geometry exposed on both sides of the N-S trending Deildargil valley. On the east outcrop, the ~2m thick inclined sheet-like body propagates through conglomerate. On the west outcrop, it follows the lower boundary of a welded ignimbrite overlaying the conglomerate unit (Fig. 4). It also cut as a dyke through a basaltic lava towards the northern end of the area.

## 4. Comparative results

An overview of the four intrusions is presented in Table 1.

**TABLE 1. DESCRIPTION OF INTRUSIONS**

| Field site | UTM | Paleodepth (m) | Intrusion type | Dip ° | Thickness (m) | Country rock type | Undamaged rock strength (MPa) |
|---|---|---|---|---|---|---|---|
| **Njarðvík-Dyrfjöll – Landsendi outcrop** | 65°33'55.75N 13°48'58.93W | 500 | Lens-shaped sill | 10-20 | 1-4 | Basalt lava | 90 |
| **Krafla – Hranftinnuhryggur outcrop** | 65°41'13.62N 16°43'40.42W | 90-40 | Steep conduit | 80 | 3-7 | Hyaloclastite | 15 |
| **Húsafell West outcrop** | 64°41'23.27N 20°57'20.85W | 500 | Irregular sheet | 45 curving to 05 | ~ 2 | Welded ignimbrite | 115 |
| **Húsafell East outcrop** | 64°41'25.78N 20°57'16.44W | 500 | Sill | 10 | ~ 2 | Conglomerate | 05 |

Note: Emplacement depth estimated from topography and literature (Burchardt, 2008; Tuffen and Castro, 2009; Mc Gowan, 2016).
Undamaged country rock uniaxial compressive strength is estimated using our Schmidt hammer data adjusted with reference to values by Eggertsson (2019).

### 4.1 The intrusions

#### *4.1.1 Landsendi (Njarðvík-Dyrfjöll)*

Orientation measurements of the contact and vesicles, and intrusive geometry of the sill tip at Landsendi, are consistent with a sill propagating towards the NE at a low discordant angle of <30° (Fig.2A). Zones of high vesicularity are associated with a higher dip in vesicle orientations and located at the sill tip or adjacent to major faults (Fig.2B). Sill thickness abruptly decreases towards the tip cavity, and the intrusion roof is displaced by several sub-vertical faults, into which rhyolite flow banding is deflected. Near the middle of the outcrop, an additional scree-hidden fault corresponds to an elevation difference of a few metres between the southern and the northern sections (Fig.2B). The rhyolite at the contact with country rock is colour-banded and contains spherulites (Figure S2. Supplemental material). A strongly fractured, friable, clay-rich layer is located at the inner marginal zone, between devitrified margins and intrusion core. These platy joints become progressively denser towards the coherent rhyolite at the sill core.

#### *4.1.2 Hrafntinnuhryggur (Krafla)*

We characterise two parts of the Hrafntinnuhryggur feeder dyke: (1) its farthest southern extent and deepest dissection (90 m), where the dyke is ~2 m thick and cuts through basalt; (2) its shallower dissection (30-50 m) 150 metres to the north, where the ~7-m-thick intrusion penetrates massive to crudely bedded basaltic hyaloclastite and flares upwards and northwards to form the columnar-jointed base of associated lava (Fig. 3). In the near-complete obsidian sheet, micro-crystalline and/or devitrified rhyolite is locally but rarely present, although predominant in the overlying dyke-fed lava bodies (Fig. 3C; Tuffen and Castro, 2009). Vesicle orientations within the intrusion show neighbouring opposite dipping directions, and flow complexity is also highlighted by a layer of hyaloclastite subdividing the intrusion in two parallel sections at the deepest dissection (Fig. 3C). Dense glass progressively transitions to highly vesicular glass towards the intrusion margins, then to pumice breccia at the contact with country rocks. This breccia consists of fibrous, tube-like pumices (0.1-10 cm), rare lithic clasts (<3 cm) and dense glassy particles (<1 cm; Fig. 7F).

#### *4.1.3 Húsafell*

A complex intrusive architecture is present at Húsafell (Fig.4D). Due to the strong similarity in intrusion dimensions and textures, and to the progressive continuity in orientations, we assume that intrusive segments along the valley are all parts of one single intrusion separated by a scree-buried fault zone (Fig.4A). At the western outcrops, an intrusive finger is present underneath the rigid layer of welded ignimbrite. Another finger cuts through it, resulting in a step-wise transgressive sill which follows the tuffisite veins. Two metres above the top contact, a >50 cm thick, near-horizontal tuffisite vein cuts friable, less densely-welded ignimbrite and extends over many tens of metres (Fig.4B). A few major faults cut through the valley, displacing many of the

studied formations (Fig.4A). The horizontal tuffisite is therefore probably connected with the intrusion at depth, but erosion has removed any evidence for a connection. Quenched margins at the contact are irregular in thickness, especially at the east outcrop where their fingering into the conglomerate follows fine-grained zone and deviates around coarser zones (Fig.4C). We use the northern section to illustrate features that are of better quality than at other localities, although it is not part of outcrops characterised for this study.

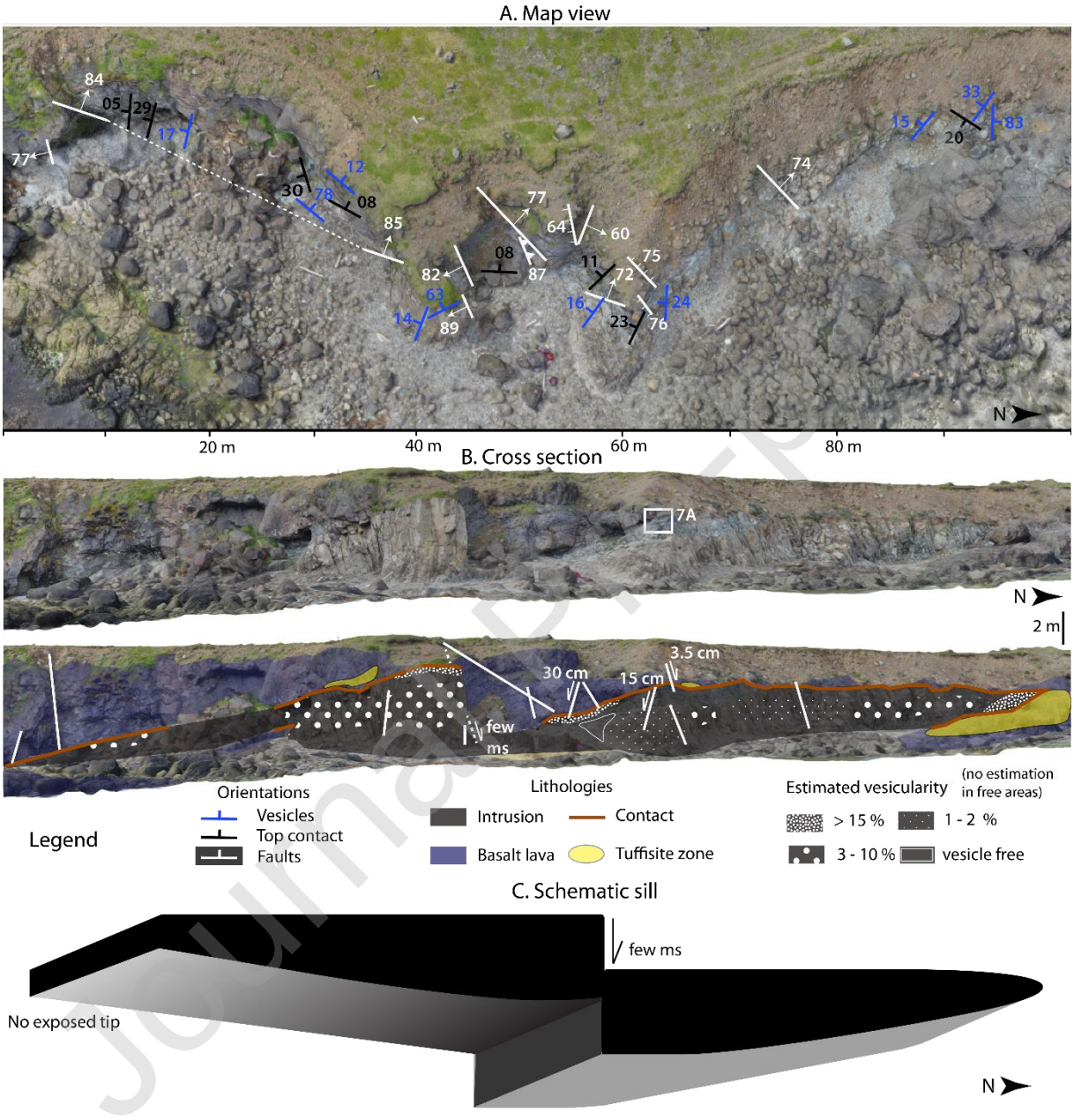


**Figure 2.** Landsendi 1-4 m thick sill in the Njarðvík-Dyrfjöll volcano. A) Map view of the intrusion with orientation of contacts, faults and vesicles. Vesicles in the intrusion core dip at 14-33°, and >63° at intrusion margins. B) Photograph (top) and interpreted (bottom) cross-section of the intrusion with vesicularity estimations, faults and areas containing tuffisites. Location of Fig. 7A is indicated by a white box. Some faults displace the sill by a few cms to >2 m. The cross section corresponds to the area in A, with horizontal-vertical scale difference caused by the perspective. C) Three-

dimensional sketch of the intrusion, based on 3D photogrammetry and field insight into top and bottom contacts. The schematic is simplified to roughly highlight the intrusion shape.

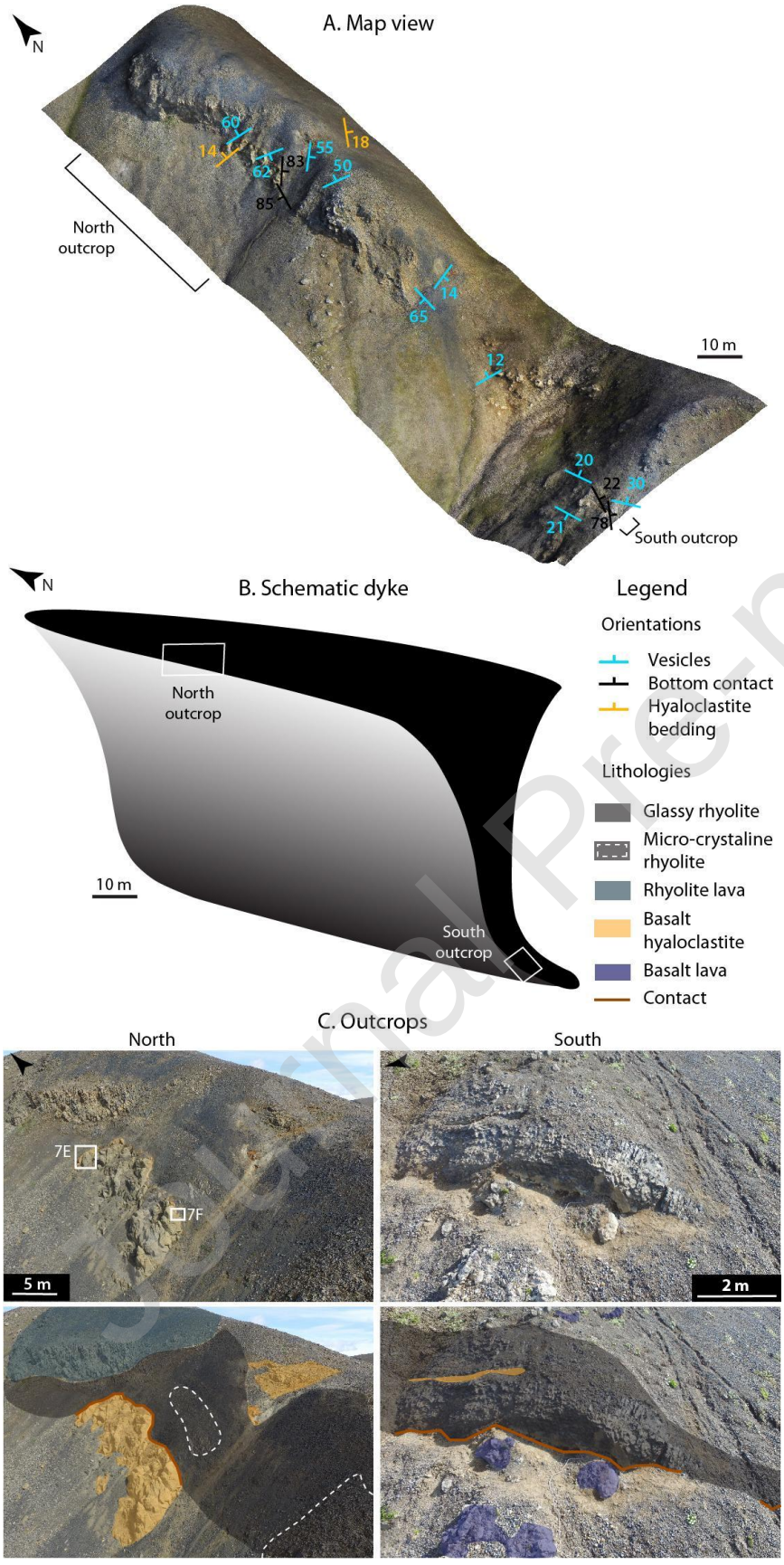

**Figure 3**. Feeder dyke at the south of Hrafntinnuhryggur, Krafla. A) Map view from photogrammetry reconstruction, with orientations of intrusion margins, hyaloclastite bedding and vesicles within the intrusion. B) Simplified 3D sketch of the dyke geometry, with location of the two outcrops. The scale is roughly similar to the map in A. C) Photograph (top) and interpreted (bottom) cross sections of north and south outcrops, with location of pictures for Figs. 7E, 7F. Change in scale from A is caused by perspective effect.

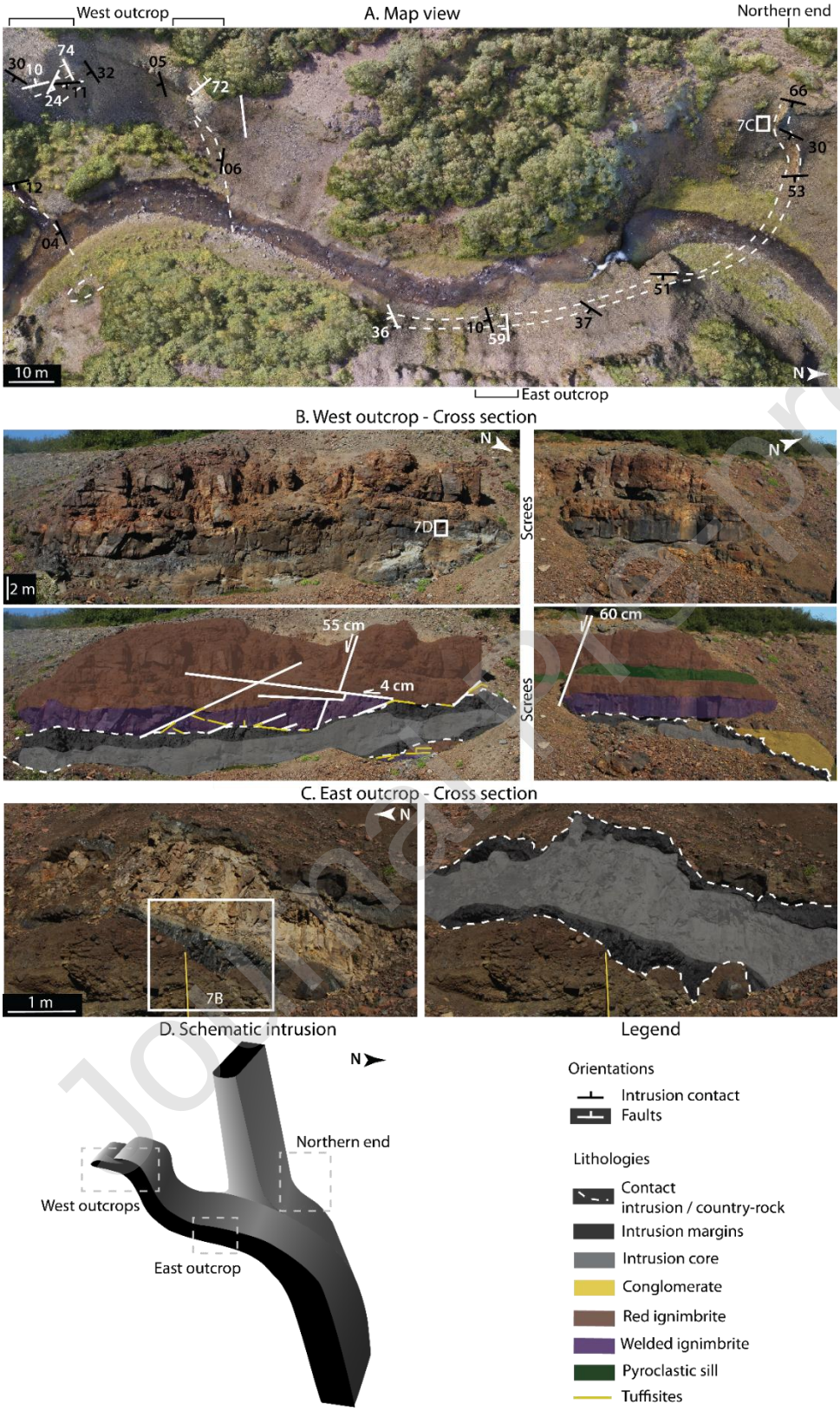

**Figure 4**. Intrusive system at Deildargil, Húsafell. A) Map view constructed from photogrammetry with orientation of intrusive contacts and faults, location of main outcrops and picture from 7C (white box). B) Photograph (top) and interpreted (bottom) cross section of Húsafell West, with highlighted faults and lithologies, and location of picture for Fig. 7D. 15 m scree-covered metres separate the lateral pictures. C) Photograph (left) and interpreted (right) cross section of rhyolite intrusion through conglomerate at Húsafell East, with location of picture for Fig. 7B. D) Simplified 3D geometry of the ~2 m thick intrusion. Not to scale.

### *4.1.4 Textures and vesicles in intrusions*

We now present the textural features of all the intrusions collectively to illustrate commonalities and distinctions.

All micro-crystalline cores are fine-grained, consisting of quartz and feldspar with ~1 mm long phenocrysts (Fig. 8C). They sharply transition towards glassy quenched margins, which exhibit a colour gradient from dark blue or green to black (Fig. 7B). Margins consist of dense and nearly crystal-free obsidian (~3% quartz and feldspar phenocrysts), locally devitrified (containing spherulites and/or lythophysae, Fig. S2) and with green amygdales (secondary mineral precipitation within cavities. Figs. 7A; 8B). They are also cut by columnar joints, sub-parallel curviplanar fractures and perlitic cracks (Fig. 8A), and progressively alter to clay minerals in zones of high fracture density.

Estimated vesicularity in all the intrusions is ≤5-10 % at cores, increasing towards intrusive tips and margins. However, the three field sites show major differences in vesicle size and shape, plotted in Fig. 5 with relative distance from the intrusion tip for localities of Landsendi and Húsafell West. The lines defined by data for small vesicles are artefacts caused by the measurement resolution.

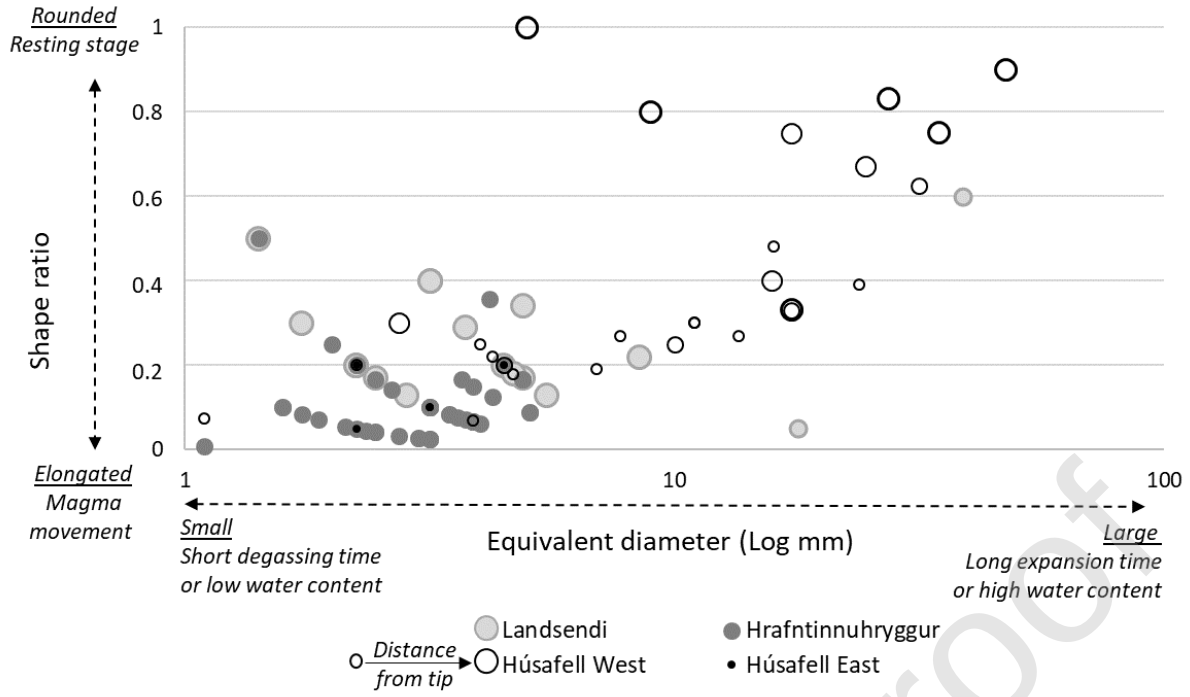


**Figure 5**. Vesicle size and shape ratio within the intrusions. Each data point represents the largest vesicle in a zone (sill tip, roof, core and bottom of intrusion. c.f. Supplemental material Fig.S1 and Table S3). Data from the sill tip at Landsendi are represented with smaller dots and data at Húsafell West are divided into 4 zones: sill tip (smallest dots), 1.5 m away, 5.5 m away and 8.5 m away from the sill tip (largest dots).

At Landsendi, vesicles are small (mean 7 mm in equivalent diameter) and elongate (average shape ratio 0.3). The two largest vesicles were both measured at the sill tip. At Hrafntinnuhryggur, vesicles are smaller (mean 3 mm) and have the lowest shape ratio at 0.1 (highly elongate), with decreasing shape ratio for increasing vesicle size. At Húsafell West, vesicles are the largest (12 mm) and have the highest shape ratio of 0.4 (most spherical). However, vesicle shape ratio decreases towards the intrusive tip, from >0.8 to <0.4, as vesicles become progressively more elongate. The shape ratio also increases with vesicle size, as largest vesicles are the most spherical. At Húsafell East, vesicles are small (3 mm) and strongly elongate (shape ratio <0.2), similar to Hrafntinnuhryggur vesicles, although there is no discernible trend.

### 4.2 The intrusion-country rock interface

The intrusion-country rock interface (logged for each site on Fig. 6) highlights that rhyolite is systematically chilled at the contact. Fig. 7 shows associated features of particular interest, and lithologies are pictured in Fig. 8. We observe stratigraphic differences for each site, which can nevertheless be paired: At Landsendi and Húsafell West, tuffisite breccia separates the intrusion from the country rock (Fig. 7D) and tuffisite veins propagate into the country rock (Fig. 7C). At

Hrafntinnuhryggur and Húsafell East, the rhyolite is directly in contact with the country rock, which shows a colour variation (Fig. 7B, E, F).

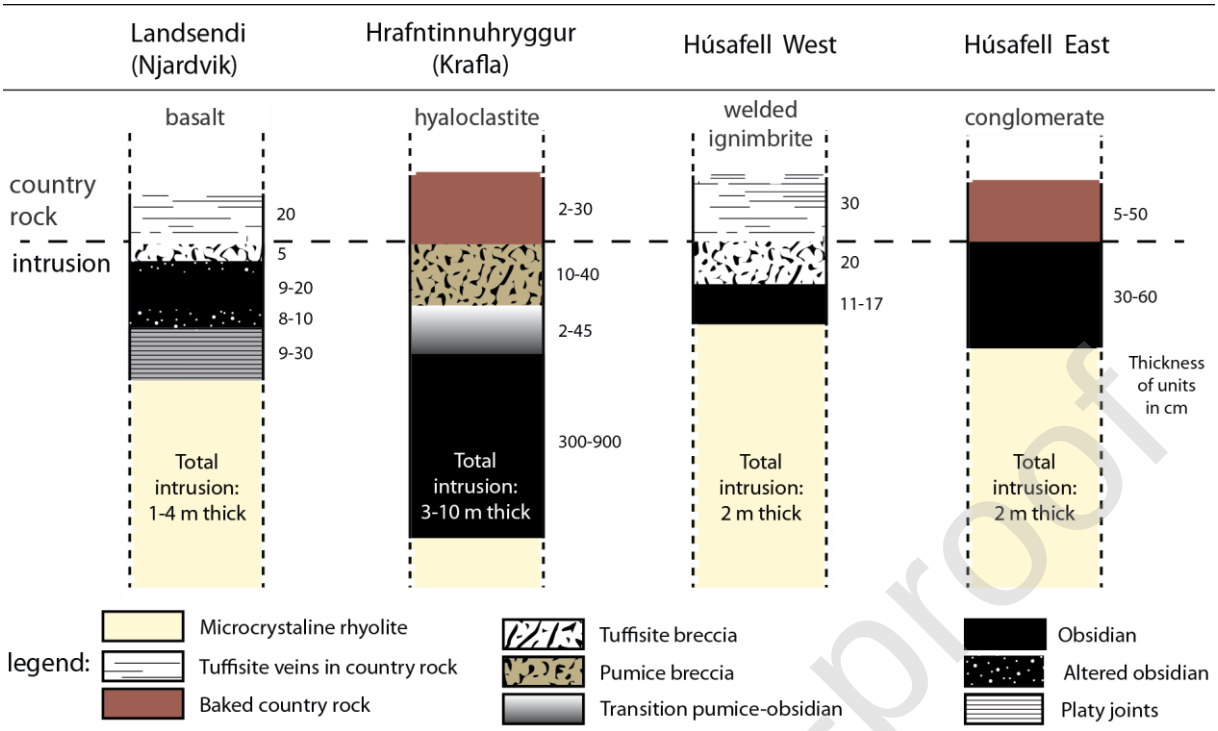


**Figure 6.** Geological logs of intrusion-country rock interfaces. Thickness given next to each unit is in cm. Country rocks are either baked (hyaloclastite at Hrafntinnuhryggur and conglomerate at Húsafell East) or brecciated and fractured (basalt at Landsendi and welded ignimbrite at Húsafell West). Damage zone thickness is estimated from macro-scale visible indicators, and so are minima as micro-scale alteration is likely more extensive.


**Figure 7**. Intrusive materials and country rocks. Contacts are outlined with a white dashed line. A) Platy zone at Landsendi, in between devitrified obsidian and rhyolite core in the intrusion. B) Húsafell East. Directly at the contact, rhyolite is quenched and conglomerate is baked. C) Tuffisite veins (contours in back line) cutting through basalt at the northern end of Húsafell site. D) Húsafell West. Tuffisite breccia between rhyolitic glass and ignimbrite. E) Hyaloclastite at Hrafntinnuhryggur, with colour gradient towards the contact. F) Pumice breccia at the contact with hyaloclastite at Hrafntinnuhryggur.

### *4.2.1 Landsendi – Basalt*

Undamaged basalt lava units at Landsendi are exposed in irregular ~3 m-thick sheets with poorly vesicular coherent dense core and ~5 mm long feldspar phenocrysts (Fig. 8D). Damaged basaltic lava (Fig. 8H) has vesicles filled with green amygdales and contains fractures exploited by tuffisite

veins a few millimetres to ~10 cm wide (similar to Fig. 7C). In the immediate vicinity of the intrusion, fracture density increases. At the northern sill tip, erosion exposes a ~10 $m^2$ surface of underlying basalt covered by an irregular layer of 5 cm-thick tuffisite breccia (Fig. 2B). At the intrusion roof, similar breccia appears as local ~20 cm long patches, at one occasion associated with a syn-emplacement fault (Fig.2B). The tuffisite veins are in general filled by predominantly well-sorted, partially rounded and fine-grained (<1mm) material in complex depositional structures, with occasional coarser (1-5mm), poorly-sorted lenses or layers (similar to Fig. 7C). Clasts include lithics derived from the country rocks, juvenile pumices, glass and micro-crystalline rhyolite associated with the intrusion. Tuffisite breccias (Fig.7D) are coarser-grained equivalents of the tuffisite veins, but are finer-grained, less pumice-rich and more compacted than pumice breccia (Fig.7F).

#### *4.2.2 Hrafntinnuhryggur - Hyaloclastite*

At Hrafntinnuhryggur, Pleistocene basaltic hyaloclastite was emplaced subglacially (Tuffen and Castro, 2009) and exhibits complex bedding, which may have been deformed or displaced by the intrusion. Bedding irregularity and the rarity of outcrops prevent any systematic record of orientations (Fig. 3A). Undamaged hyaloclastite is mostly poorly sorted and pale yellowish-brown to grey. It consists of a fine-grained palagonitic matrix with heterogeneously dispersed, 1-20 cm long, angular clasts of crystalline basalt, and predominantly glassy <5 mm long clasts (Fig. 8G). Within ~40 cm of the intrusion margin, the altered hyaloclastite displays an orange colour (Figs. 7E; 8K).

#### *4.2.3 Húsafell West – Welded ignimbrite*

Undamaged welded ignimbrite from the Deildargil ignimbrite formation is a 1.6 m-thick near-horizontal sheet densely compacted into glass. It contains 4-5 cm long and >2 cm wide horizontal fiamme, rare 2 mm long, predominantly feldspathic phenocrysts, and many 1-3 cm lithophysae (Fig. 8E). The damaged welded ignimbrite is highly fractured, and these fractures have white alteration haloes <5 mm wide (Fig. 8I). Tuffisite breccias are emplaced along the intrusion margins, forming a <~5 cm thick irregular unit (Fig. 7D). Tuffisite veins cut the ignimbrite, <1 metre from the intrusion (Fig. 7C). One notable sub-horizontal vein cuts friable ignimbrite ~2 m above the intrusion, reaching ~50 cm thick and exposed over ~60 m. It contains complex sedimentary structures, with interfingering and injection into fragments of friable ignimbritic country rock at the upper and lower vein walls.

#### *4.2.4 Húsafell East – Conglomerate*

The contact intrusion-conglomerate at Húsafell East is very sharp and undisturbed by any vein or breccia, and the quenched margins follow the country rock irregularities. Undamaged

conglomerate is typically massive and poorly-sorted, but locally bedded, with a fine-grained pale grey to yellow matrix. The largest clasts are a few cm in size (Fig. 8F). The damaged conglomerate is more compact and of a browner colour with fractures extending ~10 cm from intrusion margins (Figs. 8J; 7B).

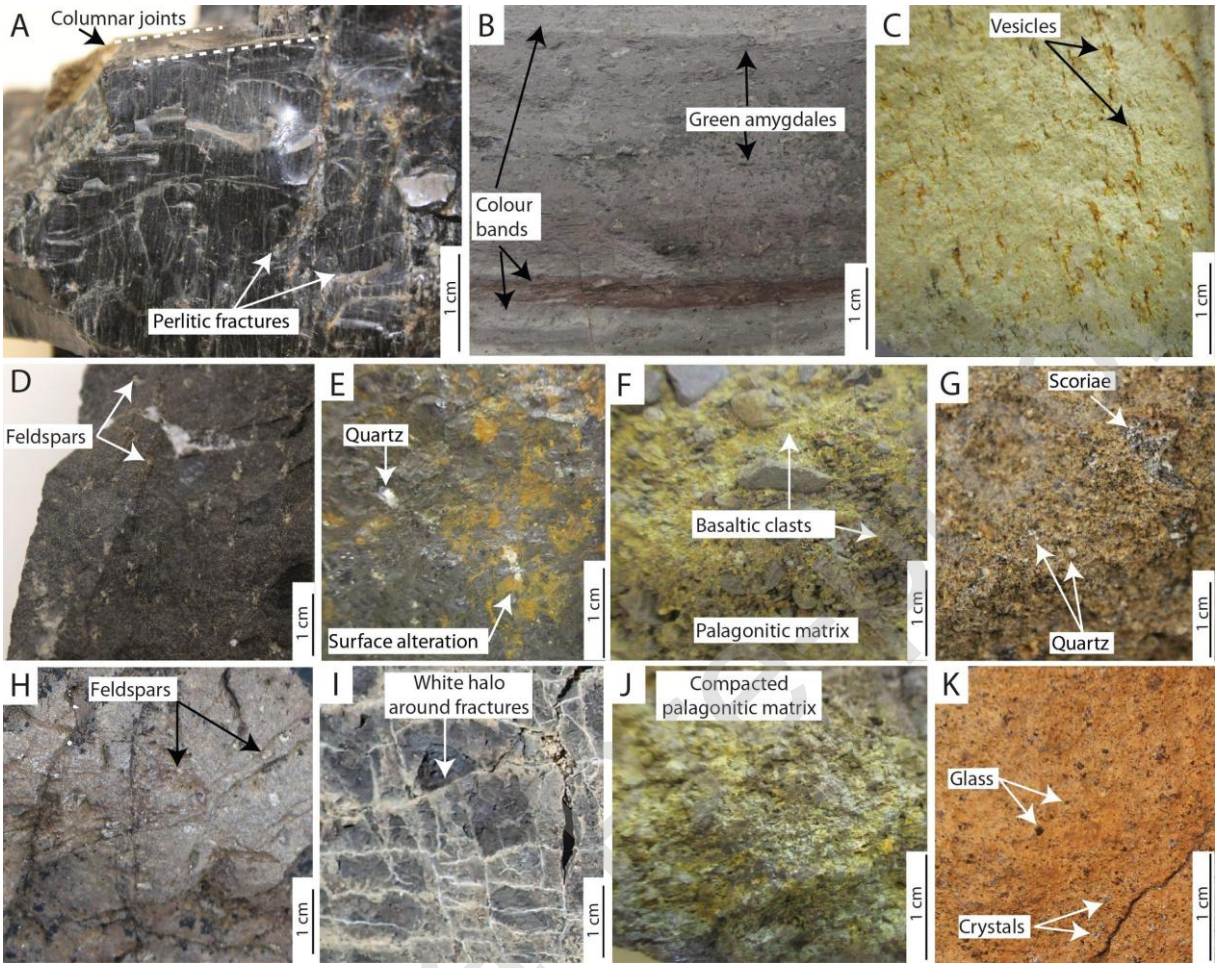


**Figure 8**. Geotechnical units. A) Obsidian from the glassy margin at Húsafell East. B) Devitrified chilled margins with colour bands at Landsendi. C) Rhyolite core from Landsendi. D) Undamaged basalt lava from Landsendi. E) Undamaged welded ignimbrite at Húsafell West. F) Undamaged conglomerate at Húsafell East. G) Undamaged hyaloclastite at Hrafntinnuhryggur with palagonitic matrix. H) Damaged basalt at Landsendi. I) Damaged welded ignimbrite at Húsafell West J) Damaged conglomerate at Húsafell East. K) Damaged hyaloclastite at Hrafntinnuhryggur.

## 4.3 The impact on country rocks

### *4.3.1. Geotechnical units*

We sort the lithologies into 11 geotechnical units according to the classification by del Potro and Hurliman (2008), illustrated in Figure 8 and briefly described in Table 2: Rhyolite intrusions are subdivided into obsidian margins (Fig.8A), clay-rich altered zones (Fig.8B) and crystalline cores (Fig.8C). Country rocks include undamaged basalt lava (Fig.8D), welded ignimbrite (Fig.8E),

conglomerate (Fig.8G), hyaloclastite (Fig.8I) and their damaged equivalents (Fig.8F, 8H, 8J, 8K, respectively).

**TABLE 2. GEOTECHNICAL UNITS**

| Geotechnical unit | Location | Alteration/damage state (sub-unit) | Description |
|---|---|---|---|
| Rhyolite - Crystalline core | All sites | Fresh | Very fine-grained with feldspar phenocrysts (masses of feldspar, $SiO_2$ polymorphs and oxides). Low vesicularity. |
| Rhyolite - Obsidian margins | | Fresh | Near crystal-free perlitic obsidian with variable vesicle content. Colour bands. |
| Rhyolite | | Altered | Strongly devitrified and commonly further altered to an assemblage of clay minerals. |
| Basalt lava | Landsendi | Undamaged | Coherent dense core poorly vesicular, finely crystalline groundmass with feldspar phenocrysts. |
| | | Damaged | As above but cut by fractures and tuffisite veins. Vesicles filled with green alteration minerals. |
| Hyaloclastite | Hrafntinnuhryggur | Undamaged | Poorly sorted with angular, glassy and crystalline lava clasts cemented in a fine-grained palagonitic matrix. Brown-grey. |
| | | Damaged | Orange colour. Fractures < 20 cm long. |
| Welded ignimbrite | Húsafell West | Undamaged | Densely welded, nearly porosity-free glassy ignimbrite with distinctive near-horizontal elongated fiamme. Contains 2 mm phenocrysts and 1-3 cm lithophysae. |
| | | Damaged | Highly fractured, with white alteration halo. Cut by tuffisite veins. |
| Conglomerate | Húsafell East | Undamaged | Massive, poorly-cemented polymictic conglomerate with grey to yellow weakly palagonitised matrix and prominent rounded basaltic clasts. Local better-sorted, bedded lenses. |
| | | Damaged | As above but fractured, with a yellow to brown or red matrix. |

### *4.3.2 Field assessment of rock properties*

Tinyperm and Schmidt hammer measurements of permeability and relative hardness are presented in Figures 9 and 10, respectively. Measurements extend 1.4-3.2 m from the contact into the country rock, with 4-15 measurement points per transect. The permeability increase towards the contact in the damaged basalt and welded ignimbrite is > 1 order of magnitude over ~30 cm, which does not exceed the variability in the undamaged country rock, and is not statistically significant. The variability in undamaged conglomerate and hyaloclastite is smaller (~half an order of magnitude, Fig. 9; Eggertson et al., 2018) and permeabilities decrease towards the intrusion by >1 order of magnitude over 20-40 cm, from $5{\cdot}10^{-13}$ to $10^{-14}$ and $5{\cdot}10^{-12}$ to $10^{-13}$, respectively. These variations thus exceed that of the variability in undamaged rocks and the significance is confirmed by the ANOVA statistical analysis of the results (p-values < 0.04).

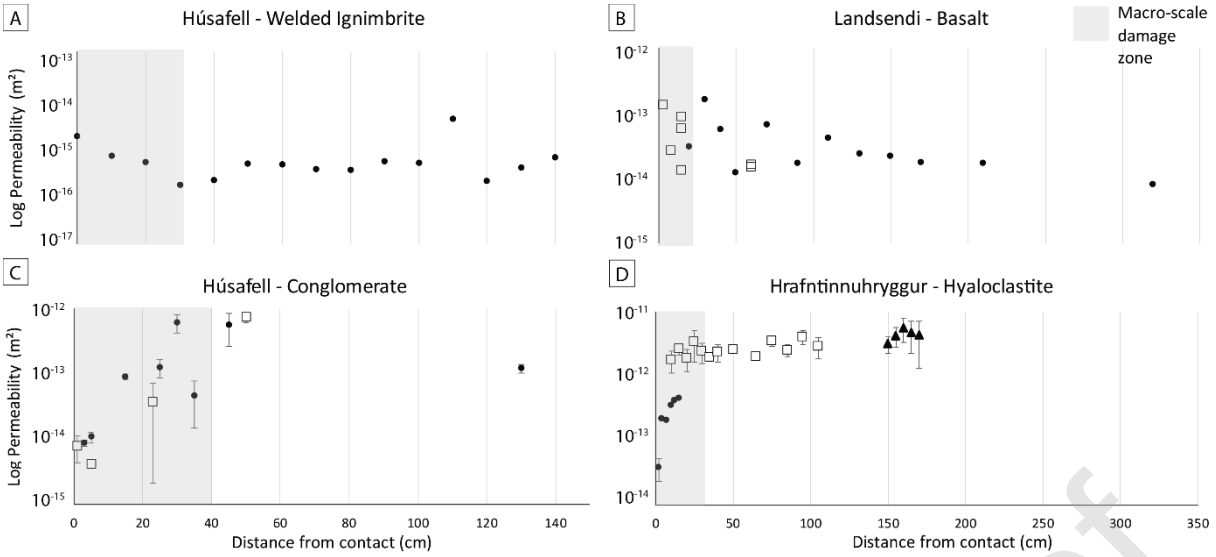


**Figure 9.** Permeability transects within country rocks. Grey areas show the extent of visible macro-scale damage at the measurement location. Each transect through the same country rock is represented by a different symbol. Error bars are one standard deviation where several measurements were made. Points without error bar were measured once (c.f. Supplemental Material, Table S1). Values have inherent uncertainties of a factor of 1.05 (Brown and Smith, 2013). A) Transects in welded ignimbrite start at the intrusion roof. B) Profiles in basalt both start at the intrusion roof. C) Profiles in conglomerate, one from the roof (squares), one from the base of the intrusion (circles). D) Profiles in the hyaloclastite at Hrafntinnuhryggur, starting at the intrusion base.

The hardness significantly decreases by a factor >2 towards the intrusion in welded ignimbrite and basalt, with the change initiated at ~60 cm and ~90 cm from the contact, respectively (Fig. 10). These distances are greater than the distance at which macro-scale damage are recorded.

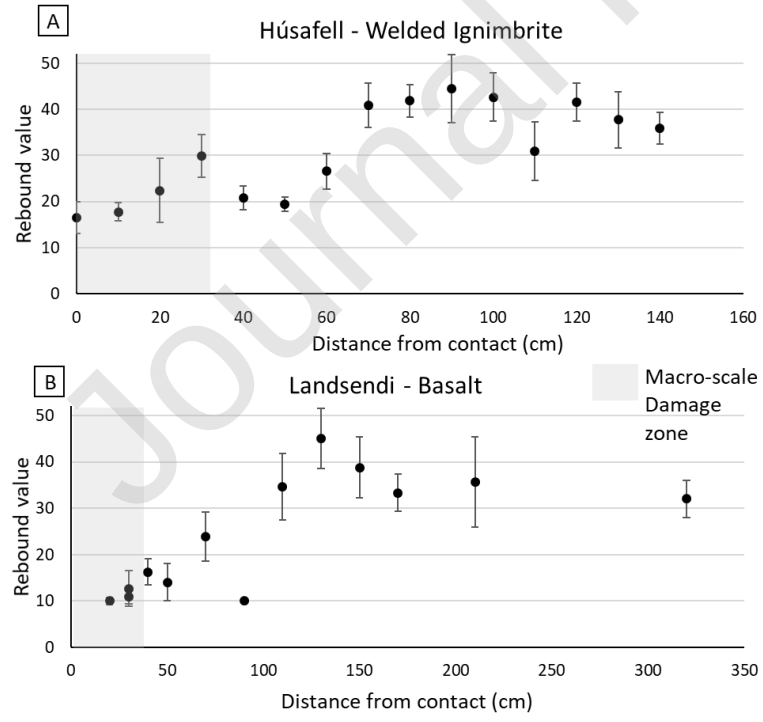

**Figure 10**. In-situ Schmidt hammer rebound along transects in the country rocks. The rebound value is proportional to rock hardness. Each point on the graph represents the average of ~10 measurements, with error bars representing one standard deviation. Grey areas show the extent of macro-scale damage at the transect location. A) Welded ignimbrite at Húsafell. B) Basalt at Landsendi. Conglomerate and hyaloclastite hardness were too low to be measured using a Schmidt hammer.

### *4.3.3 Fracture assessment*

Fracture density and area at Húsafell are plotted against distance from the contact and averaged per transect and lithology for each outcrop in Figure 11. Data are available in Supplementary material (Fig. S1, Table S2). Changes in fracturing from undamaged to damaged welded ignimbrite and conglomerate are illustrated in Fig. 11C and 11D, respectively. In undamaged country rocks, fracture density is typically 7 fractures per metre within the welded ignimbrite (at ~80 cm from intrusion) and 2 fractures per metre in conglomerate (at ~50 cm from intrusion) (Fig.11A). These values progressively increase towards the contact by a factor of 5-7 (up to 51 and ~10 fractures, respectively). In the damaged zones of the four rock types, the average fracture density systematically exceeds that of the equivalent undamaged rock while the average fracture area is smaller (Fig.11B). Fracture density is higher in undamaged basalt and welded ignimbrite (18 and 22 fractures per metre, respectively) than in undamaged conglomerate and hyaloclastite (5 and 7 fractures per metre).

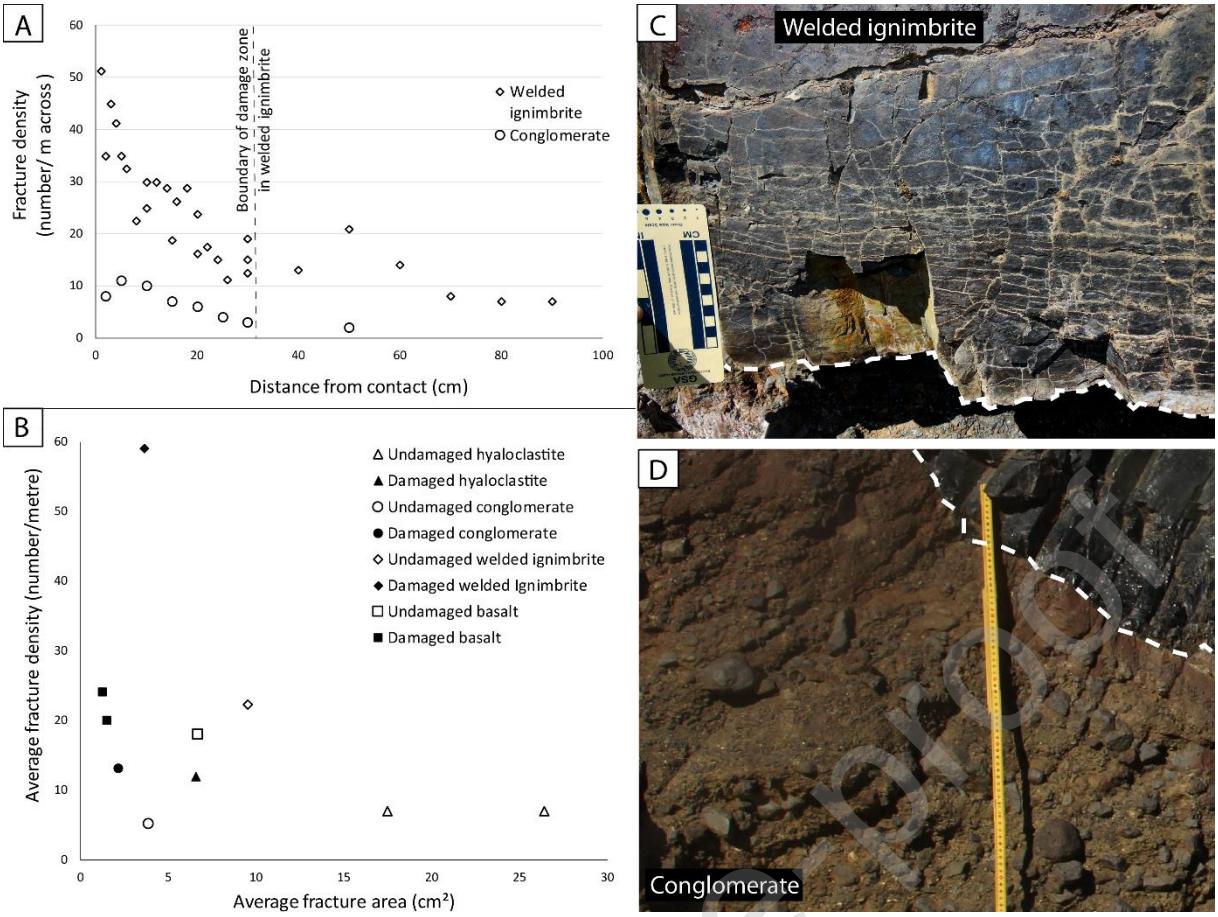


**Figure 11**. Fracture distribution in country rocks. A) Fracture density at Húsafell with distance from the intrusion. The dotted line at 30 cm corresponds to the boundary of the macro-scale damage zone in welded ignimbrite. In conglomerate, this zone is irregular, 5-50 cm thick. B) Average fracture density versus average fracture area in undamaged (empty symbols) and damaged (full symbols) country rocks. Each data point represents one set of measurements. C) Fractured welded ignimbrite at the contact (white dashed line) with the intrusion at Húsafell West. D) Fractured conglomerate at the contact (white dashed line) with the intrusion at Húsafell East.

### 4. 4 Summary of the results

At Landsendi, a sill intrudes into competent basalt lava (Fig. 8D) to form an intrusion containing stretched vesicles <15 mm long (Fig. 5) with platy jointing and devitrification of the rhyolite near the margins (Figs. 7A, 8B). The country rock is cut by tuffisite veins (similar to 7C) and by additional macro-fractures at the intrusion interface (Fig. 8H), evidenced by a slight increase in fracture density (Fig. 11B) and decreased hardness by a factor >2 (Fig. 10B).

At Hrafntinnuhryggur, a near-surface dyke intrudes through basaltic hyaloclastite and results in an obsidian intrusion with highly stretched vesicles (Fig. 5). At the margins, a progressive vesicularity gradient marks the transition towards a pumice breccia (Fig. 7F). The surrounding hyaloclastite is compact and discoloured (Figs. 7E, 8G, 8K), damaged by a few short fractures (Fig. 11B) with matrix permeability reduction of > 1 order of magnitude (Fig. 9D).

At Húsafell, a sill intrudes through conglomerate, deflecting at the base of a basalt lava and arresting at the base of a brittle welded ignimbrite, where the intrusion contains large and rounded vesicles (Fig. 5). The conglomerate at the contact is discoloured (Fig. 7B, 8J, 11D), with a slight increase in fracture density (Fig. 11) and an order of magnitude matrix permeability decrease (Fig. 9C). Where the intrusion encountered the welded ignimbrite and basalt, the interface is surrounded by tuffisite breccia (Fig. 7D) and the country rock is cut by tuffisite veins (Fig. 7C). The number of fractures in the welded ignimbrite increases by ≤7 times (Fig. 11) and the hardness decreases by a factor >2 (Fig. 10A).

## 5. Discussion

The four intrusions in this study are all rhyolitic in composition, <7 m in thickness and formed during single intrusive events in broadly similar settings and depths within Icelandic central volcanoes. They can be differentiated in terms of emplacement mechanism and influence on the surrounding rock. However, as the intrusion thicknesses—the primary factor controlling rock damage (Annen, 2017)—are broadly similar, and magma compositions lie within a restricted rhyolitic range, the mechanical response to intrusions should mostly reflect the diverse country rock type.

Direct comparison between sites have some limitations due to variation in viscosity, flow history, and fluid cooling. From their approximate paleo-depth, we estimate that water content differs by <1 wt % between the intrusions (0.3-0.4 wt. % at Hrafntinnuhryggur, Tuffen and Castro, 2009; ~1 wt. % at Húsafell, McGowan, 2016). The maximum difference in silica content is estimated ~5 wt % (~75 wt % at Hrafntinnuhryggur, Tuffen and Castro, 2009; ~72 wt % SiO2 at Húsafell, McGowan, 2016). Temperature can also vary by >100 °C for rhyolitic magmas. These parameters impact the magma viscosity, and thus the intrusive emplacement and heat transfer. Our poor control on viscosity limits interpretation for vesicle response to stress, relaxation and degassing within magma. Considering that static magma versus flowing magma also impact the heat flux (Tsang et al., in press), another limitation is the eruption-feeding dyke at Hrafntinnuhryggur, implying a flowing magma, while no conclusive evidence demonstrates whether the Landsendi or Húsafell magma erupted. An additional difference between sites is a potentially meltwater-assisted cooling at Krafla (Tuffen and Castro, 2009).

### 5.1 Emplacement processes

The intrusions in this study comprise sills, dykes, and conduits: the main types of shallow intrusions at Icelandic central volcanoes.

### *5.1.1 Landsendi*

At Landsendi, shallow dipping lava units control the intrusion shape and associated damage. The feeder system for the Landsendi sill is not visible, but the middle fault could be related to a feeder dyke or inclined sheet, which could have impacted the intrusion geometry with thickening in the central part (laccolith or lopolith; Mathieu et al., 2008; Schmiedel et al., 2017). The intrusion shape appears unaffected by regional tectonic stresses (NNE-SSW extension; Burchardt et al., 2011) and rhyolite flow banding deflection into faults at the intrusion roof indicates syn-emplacement faulting. The tuffisite breccia at the tip is emplaced against the basaltic country rock (Fig.2B), recording initial emplacement of a fragmental gas-pyroclast mixture during pathway opening. Within the intrusion, the presence of inner platy-fractured joints (Fig. 7A) is consistent with a quenching, shearing accommodation zone of outer magma during lateral propagation at high strain rates in the intrusion core. The vesicle population is small yet elongate (average 7 mm in equivalent diameter, 0.3 in shape ratio, Fig. 5), consistent with a brief phase of vesicle growth or a low water content, high shear stresses and minimal relaxation, and thus swift initial emplacement and cooling. At the sill tip, vesicles are larger and have the most extreme values in shape ratio (Fig. 5, the two >10 mm diameter vesicles, with shape ratios of 0.05 and 0.6), indicating a higher variety of vesicle processes, such as coalescence and relaxation, locally occurring together.

### *5.1.2 Hrafntinnuhryggur*

The shallow subglacial hyaloclastite environment at Hrafntinnuhryggur plays an important role in emplacement processes. High glass content and pervasive fracturing in the dyke, together with the absence of a platy-fractured zone (Fig.6), indicate rapid quenching consistent with shallow emplacement at proximity with ice. Pumice breccia is found only at this field site, the shallowest of the three, and indicates fragmentation of highly-vesicular magma prior to ascent of less-vesicular dyke-filling magma, or prior to foam collapse. The greater vesicle elongation (average shape ratio of 0.1; Fig. 5) suggests higher shear stresses than at the other intrusions, especially considering that this feeder dyke has lower water content and silica than Húsafell intrusion, and thus a lower viscosity and higher resistance to deformation for a similar temperature. The shape ratio decreases with increasing vesicle size (i.e. larger vesicles are more elongated; Fig.5) and could relate to coalescence caused by shearing during magma propagation. The magma could have had a vesicular texture similar to volcanic conduits: large, elongated vesicles on the margins and small rounded vesicles closer to the centre.

### *5.1.3 Húsafell*

The intrusion style at Húsafell particularly reflects the intruded country rock type. In the soft, weak conglomerate on the east side, the intrusion geometry is irregular. At the contact with the stronger basalt lava at the northern end, it deflects at the interface before progressing through it. When encountering the stiffer, stronger ignimbrite at Húsafell West, the intrusion forms a bedding-parallel sill periodically injecting pyroclastic material through discontinuities. The intrusion broke through the rigid country rock following the path created by pyroclastic material, propagating as a transgressive sill (Fig. 4). The thick and horizontal tuffisite vein two metres above the intrusion roof is most likely related to the opening stage of the intrusion, when over-pressured gas entered the country rock, creating a magmatic pathway. At Húsafell East, where the intrusion propagates as a sill through conglomerate, elongated vesicles (<0.2 mean shape ratio, 3mm equivalent diameter, Fig. 5) indicate rapid lateral propagation with high strain rates. At Húsafell West, where the intrusion propagates as an inclined sheet through the ignimbrite, larger vesicles (12 mm in equivalent diameter) could indicate prolonged growth during slower cooling, significant coalescence, and/or higher vesiculation triggered by higher country rock permeability (through fractures and tuffisite veins). Near-spherical vesicle shapes away from the tip and the increase in shape ratio with vesicle size (Fig. 5) are consistent with magma stalling at the encounter with the strong lithology, creating a static phase of magma relaxation and extensive vesicle growth during prolonged cooling.

### 5.2 Country rock response

Intrusive processes have both mechanical and thermal impacts on surrounding country rocks. The undamaged lithologies at our field sites consist of both weak, permeable and porous units (hyaloclastite and conglomerate) and strong, less permeable units (basalt and welded ignimbrite) (Table 1; Fig. 9). Geological logs of the contact zone and trends of permeability and hardness in the country rock reveal similarities between the response of hyaloclastite and conglomerate, and between the response of basalt and welded ignimbrite (Fig. 6; Figs. 9 and 10). These rock responses to the intrusions highlight the role of the undamaged rock properties and could in turn influence the process of intrusion emplacement.

#### *5.2.1 Interpreting permeability decrease*

Hyaloclastite and conglomerate are affected by a colour change (grey-brown to red-orange, Fig.6), pore occlusion with one order of magnitude decrease in matrix permeability (Fig.9C, 9D), a moderate increase in fracture density (7 to 12 and 5 to 13 fractures per metre, respectively; Fig. 11B), and decrease in fracture length and width (18 to 7 $cm^2$ and 4 to 2 $cm^2$ fracture area, respectively; Fig. 10B).

Thermal alteration is more pervasive in weak country rocks with originally high permeability and porosity. High-temperature fluids readily propagated through the interconnected pore network, with advection and convection potentially expanding the thermally-affected zone. Weak rocks compacted to accommodate the additional volume of the intrusion and ductile shear failure may have occurred (as demonstrated by laboratory deformation experiments on altered weak brecciated lava margin in Mordensky et al., 2019). Compaction could have destroyed evidence of pre-existing discontinuities and opened short tensile fractures, associated with larger shear fractures. Despite the slight increase in fracture density, we interpret a net pore occlusion and porosity decrease (similar to what was observed in weak, porous, altered andesite by Heap et al., 2015), resulting in decreased matrix permeability. Pore occlusion is likely a result of pore compaction coupled with precipitation of hydrothermal and alteration minerals.

Despite the focus of this study on the field scale fractures and rock properties, our observations are consistent with pervasive chemical, mineralogical, thermal and fluidal impacts in weak country rocks, similar to that observed in porous brecciated lava margins by Mordensky et al. (2018a).

### *5.2.2 Interpreting permeability increase and weakening*

Basalt and welded ignimbrite are weakened by a factor >2 (Fig. 10), with an associated increase in fracture density (18 to ~22 and 22 to 59 fractures per meter, respectively; Fig.11B), and are crosscut by tuffisite veins. Fractures are narrower and/or shorter (10 to 4 $cm^2$ and 7 to 1 $cm^2$ in fracture area, respectively; Fig.11B).

Mechanical damage dominates in the originally strong country rocks, with accordingly low permeability and porosity (similar to the mechanical damage in the strong, low permeability dense coherent lava and andesite intrusions in Mordensky et al., 2018a, b). Compared to the hyaloclastite and conglomerate, the fracture density of the welded ignimbrite and the basalt are always higher, revealing brittle deformation. Pre-existing fractures may have been exploited by gas and fragmented magma at the onset of magma propagation, creating the tuffisite veins (as also observed by Stasiuk et al., 1996). These veins were then used as a path for coherent magma ascent, which followed the gas and widened the tuffisite veins into intrusions. Many new fractures were also created, as demonstrated by the lower hardness and high fracture density close to the intrusion (Figs. 10, 11), while matrix permeability was not significantly affected (Figs. 9A, 9B). However, considering the large amount of fractures at the interface, especially in welded ignimbrite, and the significant decrease in hardness in both rocks, the rock mass permeability in these units likely increases (as in Heap and Kennedy, 2016) towards the intrusions (as observed in originally strong, dense coherent andesite lava and intrusive by Mordensky et al. 2018a).

We have no evidence for chemical, mineralogical or thermal alteration of these strong country rocks, but the intense fracturing suggests the generation of rock mass permeability that is favourable for hydrothermal fluid circulation. Any alteration occurring had a secondary impact compared to mechanical damage.

### 5.3 Overview and implications

We combine our results and field observations (rock properties, geological logs, contact features, vesicle characteristics) into one conceptual model per field site in Fig. 12, highlighting the emplacement geometry, features indicating intrusive propagation style, and impact on country rocks.

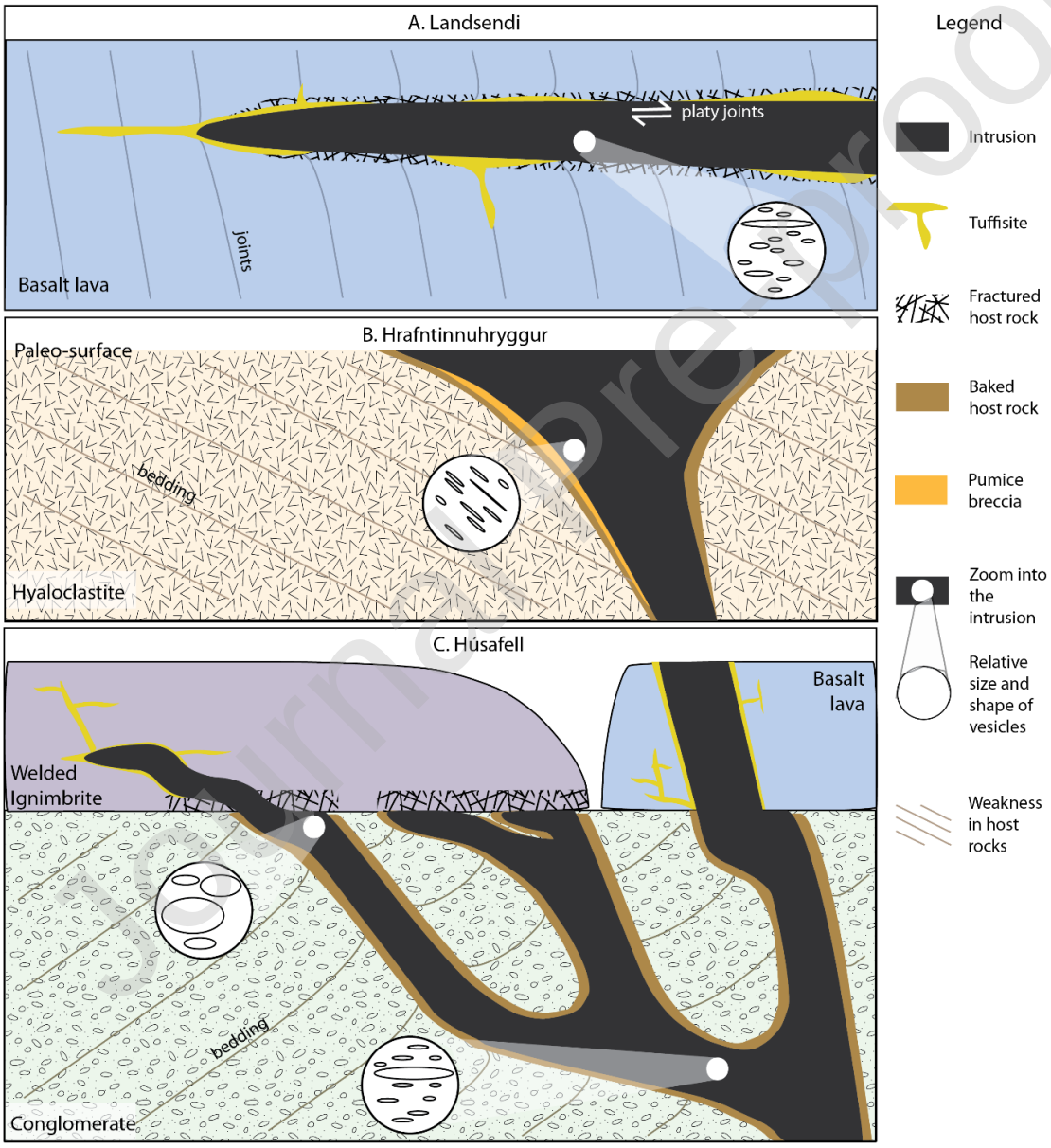


**Figure 12**. Conceptual models of the intrusions emplaced at 100–500 m depth and their contact features, at the three field sites in Icelandic central volcanoes. Schematic cross-sections are based on results and field observations. Vesicle

shapes and relative sizes are indicated within the white circles. Not to scale. A) 1-4 m thick sill at Landsendi. Magma emplaced along a fracture network filled with tuffisite veins. Remnant tuffisite breccia is irregular along the contacts with fractured basalt and a few veins cut through the country rock. Rapid lateral propagation induced high strain rates during magma emplacement, which highly deformed the vesicles. High stress and slow cooling create platy jointing within the intrusion, between the quenched margins and micro-crystalline core. B) 3-7 m thick feeder dyke at Hrafntinnuhryggur. Shallow emplacement depth permitted rapid magma decompression, leading to vesiculation, vesicle shear, and formation of pumice at dyke margins. Hyaloclastite at the contact is altered with colour change, pore occlusion and a few tensile fractures. C) 2 m thick intrusion forming a network of dykes and sills at Húsafell. Conglomerate inelastically accommodates magma propagation, resulting in colour change, pore occlusion and opening of small tensile fractures. Within the magma, vesicles are sheared according to the propagation direction. The intrusion is deflected at the base of stronger basalt lava, but cut through it, emplacing along tuffisite breccia in a similar process to what occurred at Landsendi. Because this section was not characterised in details, variation in fracture population is unknown. The intrusion fractures the base of strong welded ignimbrite, but could have initially failed to intrude it, with repeated attempts creating several intrusive fingers. Magma stalling allows vesicle relaxation into rounded shapes, and the melt eventually propagated into the ignimbrite following tuffisitic patterns.

Transposing the models at deeper emplacement and higher confining pressure, we would expect less magma degassing and lower permeabilities in the country rock. Magma vesicularity could be lower and material, fluid and gas injection into country rock as tuffisite veins, or magmatic fluids, would be restricted. Country rock fracturing would also be increasingly influenced by lithological pressure and more dominated by local tectonics. Ductile deformation is likely to dominate below ~7-9 km (Greenfield and White, 2015), although this may be locally shallower associated with more porous altered rocks (Mordensky et al 2019) and hydrothermal reservoirs and rhyolitic intrusions are commonly found significantly shallower in Iceland (e.g. Weber and Castro 2017).

Damaged and altered country rocks are the origin of every overlying hydrothermal system. Their rock properties influence the mode of heat transfer and fluid circulation, and thus hydrothermal system architecture. There is no major variation of matrix permeability between different types of damaged country rocks (~1 order of magnitude difference, Fig. 9), but high fracture density in rocks responding by weakening suggests a jump in rock mass permeability. Hydrothermal fluids could propagate in a channelized way through the discontinuities, in contrast to a matrix permeability clogging through pore occlusion. Resulting convection and advection of heat and fluids could increase the rate of heat transfer through damage zones, causing a more dynamic hydrothermal system. These more permeable rock masses (as shown in Heap and Kennedy, 2016) could thus make them viable for geothermal fluid extraction, possibly acting as feed zones. We consequently propose that the initial mechanical properties of intrusion-hosting rocks are an important consideration for geothermal exploration and reservoir engineering.

Forecasting of silicic magma mobility at caldera complexes relies on interpretation of deformation and seismic data, and therefore also directly relates to the deformation response of intruded

country rock. The strong dependence of intrusion-triggered compaction and fracturing on the initial properties of the country rock highlights the importance of robust characterisation of the mechanical properties of caldera-filling formations, to enable appropriate geophysical data interpretation.

## 6. Conclusions

This study highlights how country rock response to shallow intrusion of silicic magma can vary. Icelandic rhyolitic intrusions were characterised at three field sites and within four country rock lithologies. Results are relevant within the context of Icelandic central volcanoes and shallow magma bodies, above the crustal ductile/brittle transition zone.

At Landsendi, the emplacement of a 1-4 m-thick rhyolitic sill into basaltic lava involved a dynamic lateral propagation, as indicated by tuffisite veins and breccia, platy jointing and elongated vesicles. Basalt at the contact is fractured over ~20 cm and its hardness is decreased by a factor >2.

At Hrafntinnuhryggur, Krafla, a shallow, 3-7 m-thick eruption-feeding dyke contains highly-elongated vesicles. Upward dyke widening and the presence of pumice breccia reflect the shallow degassing of an erupting magma. Basalt hyaloclastite at the contact is discoloured over <30 cm and fractured, with a decrease in matrix permeability by >1 order of magnitude.

At Húsafell, magma ascent within a complex ~2 m-thick rhyolitic sheet was stalled by encounter with strong welded ignimbrite, generating multiple sill tips and large, rounded vesicles in stalled magma that relaxed during prolonged cooling. Welded ignimbrite is highly fractured over 30 cm at the contact and its hardness is decreased by a factor >2. Lateral propagation in the underlying conglomerate resulted in an irregular <50 cm thick discoloured zone in the country rock, crossed by rare short and narrow fractures and corresponding to ~1 order of magnitude decrease in matrix permeability.

We propose a bimodal response behaviour to intrusive processes, based on observed damage and alteration in country rocks which relate to their initial properties, and impact the propagation style:

- Rock response by pore occlusion: in originally weak, porous and highly-permeable conglomerate and hyaloclastite (estimated initial UCS <15), porosity reduces by compaction and/or mineral precipitation, and permeability decreases accordingly by >1 order of magnitude. The inelastic accommodation to magma propagation allows irregular intrusive geometries to form.

- Rock response by weakening: in initially strong, low-permeability basaltic lava and welded ignimbrite (estimated initial UCS >90), intense fracturing and exploitation of fractures by tuffisite veins weaken the rock by a factor >2. These rocks appear to require accumulation of magmatic pressure with systematic formation of tuffisite veins prior to intrusive emplacement.

Our field observations of intrusion-country rock interactions provide critical information about the process of silicic magma ascent in the shallow crust and country rock response. Similar knowledge of geothermal reservoir formations will additionally shed useful light on evolving geothermal resources within intruded geothermal systems. Similarly, such a knowledge of caldera-filling formations will help the forecast of magma mobility.

## Author contributions

The study was devised by ES, BK, HT and MV. Manuscript preparation was led by ES with the inputs and reviews of all the authors. Figures were drafted by ES with contributions from JD. The Njarðvík-Dyrfjöll site was introduced by SB, and Hrafntinnuhryggur and Húsafell by HT. All the authors carried out the fieldwork: ES, BK and MV performed scanline transect measurements; ES and HT measured vesicle properties; ES and JD carried out virtual coverage with the remote aircraft combined with high quality hand-camera pictures from BK and HT; Faults were recorded by SB, ES and HT; all the authors contributed to rock properties measurement with the TinyPerm and Schmidt hammer, and to the measurements of features orientation and dimensions. Data analysis was performed by ES and interpretations built with contributions from all the authors. Statistical analysis was conducted by ES.

Declarations of interest

none

**Declaration of interests**

The authors declare that they have no known competing financial interests or personal relationships that could have appeared to influence the work reported in this paper.

The authors declare the following financial interests/personal relationships which may be considered as potential competing interests:

## Acknowledgements

The authors thank the National Power Company of Iceland (Landsvirkjun) for the accommodation provided at Krafla. We are also thankful to Felix von Aulock (University of Liverpool, UK) and Einar Bessi Gestsson (Uppsala University and Icelandic Meteorological office) for their assistance on the field, and to the farmers at Njarðvík for kindly giving access to the field sites. This work was supported by the Ministry of Business, Employment and Innovation, New Zealand [grant number E6552]; the Mason Trust funding from the University of Canterbury, New Zealand; and a Royal Society University Research Fellowship to HT.

## References

Annen, C. 2017. Factors Affecting the Thickness of Thermal Aureoles. Frontiers in Earth Science, 5.

Albertsson, A., Bjarnason, J. Ö., Gunnarsson, T., Ballzus, C., & Ingason, K., 2003. The Iceland Deep Drilling Project: Fluid Handling, Evaluation, and Utilization, 8.

Arnórsson, S., Axelsson, G., & Saemundsson, K., 2008. Geothermal systems in Iceland. Jökull.

Amaral, P.M., Rosa, L.G., Fernandes, J.C., 1999. Determination of Schmidt rebound hardness consistency in granite. International Journal of Rock Mechanics and Mining Sciences, 36, 833 – 837.

American Society for Testing and Materials, 2001. Standard test method for determination of rock hardness by rebound hammer method. ASTM Standard. 04.09 (D 5873-00).

Aydin, A. & Basu, A., 2005. The Schmidt hammer in rock material characterization. Engineering Geology, 81, 1-14.

Björnsson, A., Johnsen, G., Sigurdsson, S., Thorbergsson, G., & Tryggvason, E. 1979. Rifting of the plate boundary in north Iceland 1975–1978. Journal of Geophysical Research: Solid Earth, 84(B6), 3029–3038.

Brown, S., & Smith, M., 2013. A transient-flow syringe air permeameter. Geophysics, 78(5).

Burchardt, S., 2008. New insights into the mechanics of sill emplacement provided by field observations of the Njarðvík Sill, Northeast Iceland. Journal of Volcanology and Geothermal Research, 173, 280–288.

Burchardt, S., Tanner, D. C., Krumbholz, M., 2012. The Slaufrudalur Pluton, Southeast Iceland - An example of shallow magma emplacement by coupled cauldron subsidence and magmatic stoping. Geological Society of America Bulletin, 124, 213-227.

Burchardt, S., Mattsson, T., Palma, J. O., Galland, O., Almqvist, B., Mair, K., … Sun, Y. 2019. Progressive Growth of the Cerro Bayo Cryptodome, Chachahuén Volcano, Argentina—Implications for Viscous Magma Emplacement. Journal of Geophysical Research: Solid Earth,

Carrigan, C. R., 1986. A two-phase hydrothermal cooling model for shallow intrusions. Journal of Volcanology and Geothermal Research, 28(1), 175–192.

Clemens, J. D., Petford, N. 1999. Granitic melt viscosity and silicic magma dynamics in contrasting tectonic settings. Journal of the Geological Society, 156, 1057–1060.

Conway, C., Townsend, D., Leonard, G. Wilson, C., Calvert, A., & Gamble, J., 2015. Lava-ice interaction on a large composite volcano: a case study from Ruapehu, New Zealand. Bulletin of Volcanology, 77.

Deere, D. U., Miller, R. P., 1966. Engineering classification and index properties for intact rock. Technical report, University of Illinois, Urbana, Illinois, 327p.

Delaney, P. T., Pollard, D. D., Ziony, J. I., & McKee, E. H., 1986. Field relations between dikes and joints: Emplacement processes and paleostress analysis. Journal of Geophysical Research: Solid Earth, 91(B5), 4920–4938.

Del Potro, R., & Hürlimann, M., 2008. Geotechnical classification and characterisation of materials for stability analyses of large volcanic slopes. Engineering Geology, 98(1–2), 1–17.

Dingwell, D. B., Lavallée, Y., Hess, K.-U., Flaws, A., Marti, J., Nichols, A. R. L., … Schillinger, B. 2016. Eruptive shearing of tube pumice: pure and simple. Solid Earth, 7(5), 1383–1393.

Eggertsson, G. H., Lavallée, Y., Kendrick, J. E., & Markússon, S. H., 2018. Improving fluid flow in geothermal reservoirs by thermal and mechanical stimulation: The case of Krafla volcano, Iceland. Journal of Volcanology and Geothermal Research.

Eggertsson, G. H., 2019. Constraining mechanical and permeability properties of the Krafla geothermal reservoir, North-East Iceland. PhD thesis, Liverpool University, UK.

Elders, W. A., Friðleifsson, G. Ó., Zierenberg, R. A., Pope, E. C., Mortensen, A. K., Guðmundsson, Á., … Schiffman, P., 2011. Origin of a rhyolite that intruded a geothermal well while drilling at the Krafla volcano, Iceland. Geology, 39(3), 231–234.

Farquharson, J., Heap, M. J., Varley, N. R., Baud, P., & Reuschlé, T., 2015. Permeability and porosity relationships of edifice-forming andesites: A combined field and laboratory study. Journal of Volcanology and Geothermal Research, 297, 52–68.

Farquharson, J. I., Wild, B., Kushnir, A. R., Heap, M. J., Baud, P., & Kennedy, B. 2019. Acid-Induced Dissolution of Andesite: Evolution of Permeability and Strength. Journal of Geophysical Research: Solid Earth, 124(1), 257-273.

Fisher, R. A. 1925. Statistical Methods for Research Workers (Oliver and Boyd).

Galland, O., Cobbold, P. R., Hallot, E., de Bremond d'Ars, J., Delavaud, G. 2006. Use of vegetable oil and silica powder for scale modelling of magmatic intrusion in a deforming brittle crust. Earth and Planetary Science Letters, 243(3–4), 786–804.

Galland, O., Planke, S., Neumann, E.-R., & Malthe-Sørenssen, A., 2009. Experimental modelling of shallow magma emplacement: Application to saucer-shaped intrusions. Earth and Planetary Science Letters, 277(3), 373–383.

Galland, O., Bertelsen, H. S., Eide, C. H., Guldstrand, F., Haug, Ø. T., Leanza, H. A., … Spacapan, J. B. 2018. Chapter 5 - Storage and Transport of Magma in the Layered Crust—Formation of Sills and Related Flat-Lying Intrusions. In S. Burchardt (Ed.), Volcanic and Igneous Plumbing Systems,113–138.

Galushkin, Y. I., 1997. Thermal effects of igneous intrusions on maturity of organic matter: A possible mechanism of intrusion. Organic Geochemistry, 26(11), 645–658.

Greenfield, T., & White, R. S. 2015. Building icelandic igneous crust by repeated melt injections. Journal of Geophysical Research: Solid Earth, 120(11), 7771–7788.

Gudmundsson, A., 1990. Emplacement of dikes, sills and crustal magma chambers at divergent plate boundaries. Tectonophysics, 176(3), 257–275.

Gunnarsson, B., Marsh, B. D., & Taylor, H. P., 1998. Generation of Icelandic rhyolites: silicic lavas from the Torfajökull central volcano. Journal of Volcanology and Geothermal Research, 83(1–2), 1–45.

Hamada, M., Laporte, D., Cluzel, N., Koga, K. T., & Kawamoto, T., 2010. Simulating bubble number density of rhyolitic pumices from Plinian eruptions: constraints from fast decompression experiments. Bulletin of Volcanology, 72(6), 735–746.

Healy, D., Rizzo, R., Duffy, M., Farrell, N. J. C., Hole, M. J., & Muirhead, D., 2018. Field evidence for the lateral emplacement of igneous dykes: Implications for 3D mechanical models and the plumbing beneath fissure eruptions. Volcanica, 85–105.

Heap, M. J., Kennedy, B. M., Pernin, N., Jacquemard, L., Baud, P., Farquharson, J. I., … Dingwell, D. B., 2015. Mechanical behaviour and failure modes in the Whakaari (White Island volcano) hydrothermal system, New Zealand. Journal of Volcanology and Geothermal Research, 295, 26–42.

Heap, M. J., Kennedy, B. M., 2016. Exploring the scale-dependent permeability of fractured andesite. Earth and Planetary Science Letters 447, 139–150.

Heap, M. J., Violay, M., Wadsworth, F. B., & Vasseur, J., 2017. From rock to magma and back again: The evolution of temperature and deformation mechanism in conduit margin zones. Earth and Planetary Science Letters, 463, 92–100.

Heiken, G., Wohletz, K., & Eichelberger, J., 1988. Fracture fillings and intrusive pyroclasts, Inyo Domes, California. Journal of Geophysical Research: Solid Earth, 93(B5), 4335–4350.

Holness, M. B., 2018. Melt segregation from silicic crystal mushes: a critical appraisal of possible mechanisms and their microstructural record. Contributions to Mineralogy and Petrology, 173: 48.

Huppert, H. E., & Sparks, R. S. J., 1989. Chilled margins in igneous rocks. Earth and Planetary Science Letters, 397–405.

Hutton, D. H. W., 1988. Granite emplacement mechanisms and tectonic controls: inferences from deformation studies. Earth and Environmental Science Transactions of The Royal Society of Edinburgh, 79(2–3), 245–255.

Jónasson, K., 1994. Rhyolite volcanism in the Krafla central volcano, north-east Iceland. Bulletin of Volcanology, 56(6–7), 516–528.

Kavanagh, J. L., Menand, T., & Sparks, R. S. J. 2006. An experimental investigation of sill formation and propagation in layered elastic media. Earth and Planetary Science Letters, 245(3), 799–813.

Kavanagh, J. L., & Sparks, R. S. J., 2011. Insights of dyke emplacement mechanics from detailed 3D dyke thickness datasets. Journal of the Geological Society, 168(4), 965–978.

Kavanagh, J. L. 2018. Mechanisms of Magma Transport in the Upper Crust—Dyking. In S. Burchardt (Ed.), Volcanic and Igneous Plumbing Systems, 55-88.

Kennedy, B. M., Wadsworth, F. B., Vasseur, J., Ian Schipper, C., Mark Jellinek, A., von Aulock, F. W., … Dingwell, D. B. 2016. Surface tension driven processes densify and retain permeability in magma and lava. Earth and Planetary Science Letters, 433, 116–124.

Krumbholz, M., Hieronymus, C. F., Burchardt, S., Troll, V. R., Tanner, D. C., & Friese, N., 2014. Weibull-distributed dyke thickness reflects probabilistic character of host-rock strength. Nature Communications, 5, 3272.

Lamur, A., Kendrick, J. E., Eggertsson, G. H., Wall, R., Ashworth, J. D., & Lavallée, Y., 2017. The permeability of fractured rocks in pressurised volcanic and geothermal systems. Scientific Reports, 7(1).

Le Corvec, N., Menand, T., & Lindsay, J., 2013. Interaction of ascending magma with pre-existing crustal fractures in monogenetic basaltic volcanism: an experimental approach. Journal of Geophysical Research, 118, 968–984.

Maccaferri, F., Bonafede, M., & Rivalta, E., 2011. A quantitative study of the mechanisms governing dike propagation, dike arrest and sill formation. Journal of Volcanology and Geothermal Research, 208(1), 39–50.

Magnall, N., James, M. R., Tuffen, H., Vye-Brown, C., Schipper, C. I., Castro, J. M., & Davies, A. G., 2019. The origin and evolution of breakouts in a cooling-limited rhyolite lava flow. Geological Society of America Bulletin, 131(1–2), 137–154.

Manga, M., Castro, J., Cashman, K. V., & Loewenberg, M., 1998. Rheology of bubble-bearing magmas. Journal of Volcanology and Geothermal Research, 87(1–4), 15–28.

Mathieu, L., van Wyk de Vries, B., Holohan, E. P., Troll, V. R. 2008. Dykes, cups, saucers and sills: Analogue experiments on magma intrusion into brittle rocks. Earth and Planetary Science Letters, 271, 1–13.

Mattsson, T., Burchardt, S., Almqvist, B. S. G., Ronchin, E. 2018. Syn-Emplacement Fracturing in the Sandfell Laccolith, Eastern Iceland—Implications for Rhyolite Intrusion Growth and Volcanic Hazards. Frontiers in Earth Science, 6.

McGowan, E. M., 2016. Magma emplacement and deformation in rhyolitic dykes: insight into magmatic outgassing. Ph.D Thesis, Lancaster University, UK.

Miller, J., & Rupert, G. 1997. Beyond ANOVA: basics of applied statistics. Chapman and Hall/CRC Texts in Statistical Science.

Mordensky, S. P., Villeneuve, M. C., Kennedy, B. M., Heap, M. J., Gravley, D. M., Farquharson, J. I., & Reuschlé, T., 2018a. Physical and mechanical property relationships of a shallow intrusion and volcanic host rock, Pinnacle Ridge, Mt. Ruapehu, New Zealand. Journal of Volcanology and Geothermal Research, 359, 1–20.

Mordensky, S. P., Villeneuve, M., Farquharson, J. I., Kennedy, B. M., Heap, M. J., & Gravley, D. M., 2018b. Rock mass properties and edifice strength data from Pinnacle Ridge, Mt. Ruapehu, New Zealand. Journal of Volcanology and Geothermal Research, 367.

Mordensky, S., Heap, M., Kennedy, B., Gilg, H.A., Villeneuve, M., Farquharson, J., Gravley, D., 2019. Influence of alteration on the mechanical behaviour and failure mode of andesite: Implications for shallow seismicity and volcano monitoring. Bulletin of Volcanology, in press.

Mordensky S.P., Kennedy B.M. Villeneuve, M.C., Lavallee, Y., Reichow M., Wallace P.A. Siratovich P.A. & Gravley D.M. Increasing the permeability of hydrothermally altered andesite by transitory heating, Geology, Geochemistry and Geophysics, in press.

Nielsen, G., Maack, R., Gudmundsson, A., & Gunnarsson, G. I., 2000. Completion of Krafla geothermal power plant. Proceeding World Geothermal Congress.

Okumura, S., Nakamura, M., & Tsuchiyama, A., 2006. Shear-induced bubble coalescence in rhyolitic melts with low vesicularity. Geophysical Research Letters, 33(20).

Okumura, S., Nakamura, M., Takeuchi, S., Tsuchiyama, A., Nakano, T., & Uesugi, K., 2009. Magma deformation may induce non-explosive volcanism via degassing through bubble networks. Earth and Planetary Science Letters, 281(3), 267–274.

Papale, P., Neri, A., & Macedonio, G., 1998. The role of magma composition and water content in explosive eruptions: 1. Conduit ascent dynamics. Journal of Volcanology and Geothermal Research, 87(1), 75–93.

Parmentier, E. M., & Schedl, A., 1981. Thermal Aureoles of Igneous Intrusions: Some Possible Indications of Hydrothermal Convective Cooling. The Journal of Geology, 89(1), 1–22.

Paterson, S. R., Fowler, T. K., & Miller, R. B., 1996. Pluton emplacement in arcs: a crustal-scale exchange process. Earth and Environmental Science Transactions of The Royal Society of Edinburgh, 87(1–2), 115–123.

Pennacchioni, G., Di Toro, G., Brack, P., Menegon, L., & Villa, I. M., 2006. Brittle–ductile–brittle deformation during cooling of tonalite (Adamello, Southern Italian Alps). Tectonophysics, 427(1), 171–197.

Pirajno, F., 2008. Hydrothermal Processes and Mineral Systems. Springer Science & Business Media.

Pollard, D. D. 1973. Derivation and evaluation of a mechanical model for sheet intrusions. Tectonophysics, 19(3), 233–269.

Reid, F. 1983. Origin of the rhyolitic rocks of the taupo volcanic zone, New Zealand. Journal of Volcanology and Geothermal Research, 15(4), 315–338.

Rust, A. C., Manga, M., & Cashman, K. V., 2003. Determining flow type, shear rate and shear stress in magmas from bubble shapes and orientations. Journal of Volcanology and Geothermal Research, 122(1–2), 111–132.

Saemundsson, K., & Noll, H., 1974. K/Ar ages of rocks from Húsafell, Western Iceland, and the development of the Húsafell central volcano. Jökull, (24), 40–59.

Saubin, E., Tuffen, H., Gurioli, L., Owen, J., Castro, J. M., Berlo, K., … Wehbe, K., 2016. Conduit Dynamics in Transitional Rhyolitic Activity Recorded by Tuffisite Vein Textures from the 2008–2009 Chaitén Eruption. Frontiers in Earth Science, 4.

Schmiedel, T., Galland, O., & Breitkreuz, C. 2017. Dynamics of Sill and Laccolith Emplacement in the Brittle Crust: Role of Host Rock Strength and Deformation Mode. Journal of Geophysical Research: Solid Earth, 122(11), 8860–8871.

Scott, S., Driesner, T., & Weis, P. 2017. Boiling and condensation of saline geothermal fluids above magmatic intrusions. Geophysical Research Letters, 44(4), 1696–1705.

Shea, T., Houghton, B. F., Gurioli, L., Cashman, K. V., Hammer, J. E., Hobden, B. J. 2010. Textural studies of vesicles in volcanic rocks: An integrated methodology. Journal of Volcanology and Geothermal Research, 190(3–4), 271–289.

Sigurdsson, H., 1977. Generation of Icelandic rhyolites by melting of plagiogranites in the oceanic layer. Nature, 269(5623), 25–28.

Siratovich, P. A., Sass, I., Homuth, S., & Bjornsson, A. 2011. Thermal simulation of geothermal reservoirs and laboratory investigation of thermally induced fractures. Transactions - Geothermal Resources Council, 35, 1529–1535.

Sparks, R. S. J., 1978. The dynamics of bubble formation and growth in magmas: A review and analysis. Journal of Volcanology and Geothermal Research, 3(1–2), 1–37.

Spence, D. A., & Turcotte, D. L., 1985. Magma-driven propagation of cracks. Journal of Geophysical Research: Solid Earth, 90(B1), 575–580.

Stasiuk, M. V., Barclay, J., Carroll, M. R., Jaupart, C., Ratté, J. C., Sparks, R. S. J., & Tait, S. R., 1996. Degassing during magma ascent in the Mule Creek vent (USA). Bulletin of Volcanology, 58(2–3), 117–130.

Stephens, T. L., Walker, R. J., Healy, D., Bubeck, A., & England, R. W. 2018. Mechanical models to estimate the paleostress state from igneous intrusions. Solid Earth, 9(4), 847–858,

Thordarson, T., & Larsen, G. 2007. Volcanism in Iceland in historical time: Volcano types, eruption styles and eruptive history. Journal of Geodynamics, 43, 118–152.

Toramaru, A., 2014. On the second nucleation of bubbles in magmas under sudden decompression. Earth and Planetary Science Letters, 404, 190–199.

Tsang S, Lindsay, J., Coco., G, Wysocki R. Lerner G., Rader E., Turner G., & Kennedy B., The heating of substrates beneath basaltic lava flows, Bulletin of Volcanology, in press.

Tuffen, H., & Castro, J. M., 2009. The emplacement of an obsidian dyke through thin ice: Hrafntinnuhryggur, Krafla Iceland. Journal of Volcanology and Geothermal Research, 185(4), 352–366.

Tuffen, H., & Dingwell, D. B., 2005. Fault textures in volcanic conduits: evidence for seismic trigger mechanisms during silicic eruptions. Bulletin of Volcanology, 67(4), 18.

von Aulock, F. W., Nichols, A. R. L., Kennedy, B. M., & Oze, C. (2013). Timescales of texture development in a cooling lava dome. Geochimica et Cosmochimica Acta, 114, 72–80.

von Aulock, F. W., Kennedy, B. M., Maksimenko, A., Wadsworth, F. B., & Lavallée, Y., 2017. Outgassing from Open and Closed Magma Foams. Frontiers in Earth Science, 5

Wadsworth, F. B., Witcher, T., Vasseur, J., Dingwell, D. B., & Scheu, B., 2019. When Does Magma Break? In J. Gottsmann, J. Neuberg, & B. Scheu (Eds.), Volcanic Unrest: From Science to Society, 171–184.

Walker, G. P. L., 1966. Acid volcanic rocks in Iceland. Bulletin of Volcanology, 29(1), 375–402.

Walker, G. P. L., 1974. Eruptive Mechanisms in Iceland. In L. Kristjansson (Ed.), Geodynamics of Iceland and the North Atlantic Area, 189–201.

Weber, G., & Castro, J. M. 2017. Phase petrology reveals shallow magma storage prior to large explosive silicic eruptions at Hekla volcano, Iceland. Earth and Planetary Science Letters, 466, 168–180.

Weidendorfer, D., Mattsson, H. B., & Ulmer, P., 2014. Dynamics of Magma Mixing in Partially Crystallized Magma Chambers: Textural and Petrological Constraints from the Basal Complex of the Austurhorn Intrusion (SE Iceland). Journal of Petrology, 55(9), 1865–1903.

Westrich, H. R., Stockman, H. W., & Eichelberger, J. C. 1988. Degassing of rhyolitic magma during ascent and emplacement. Journal of Geophysical Research: Solid Earth, 93(B6), 6503–6511.

Wong, T., & Baud, P. (2012). The brittle-ductile transition in porous rock: A review. Journal of Structural Geology, 44, 25–53.

Zaiontz C. (2018). Real Statistics Using Excel. www.real-statistics.com accessed May 2019